MATHEMATICAL MODELLING OF BLOOD FLOW THROUGH ARTERIES AND INVESTIGATION OF SOME PATHOLOGICAL CASES IN CARDIOVASCULAR SYSTEM USING GRAD-DIV STABILIZATION

A THESIS SUBMITTED TO
THE GRADUATE SCHOOL OF NATURAL AND APPLIED SCIENCES
OF
MIDDLE EAST TECHNICAL UNIVERSITY

BY

İSMAİL TAHİR KÖKTEN

IN PARTIAL FULFILLMENT OF THE REQUIREMENTS
FOR
THE DEGREE OF MASTER OF SCIENCE
IN
MATHEMATICS

DECEMBER 2019

Approval of the thesis:

MATHEMATICAL MODELLING OF BLOOD FLOW THROUGH ARTERIES AND INVESTIGATION OF SOME PATHOLOGICAL CASES IN CARDIOVASCULAR SYSTEM USING GRAD-DIV STABILIZATION

submitted by **İSMAİL TAHİR KÖKTEN** in partial fulfillment of the requirements for the degree of **Master of Science in Mathematics Department, Middle East Technical University** by,

Prof. Dr. Halil Kalıpçılar
Dean, Graduate School of **Natural and Applied Sciences** _____

Prof. Dr. Yıldıray Ozan
Head of Department, **Mathematics** _____

Prof. Dr. Songül Kaya Merdan
Supervisor, **Mathematics, METU** _____

Examining Committee Members:

Assist. Prof. Dr. Baver Okutmuştur
Mathematics, METU _____

Prof. Dr. Songül Kaya Merdan
Mathematics, METU _____

Assoc. Prof. Dr. Aytekin Çıbık
Mathematics, Gazi University _____

Date:

I hereby declare that all information in this document has been obtained and presented in accordance with academic rules and ethical conduct. I also declare that, as required by these rules and conduct, I have fully cited and referenced all material and results that are not original to this work.

Name, Surname: İSMAİL TAHİR KÖKTEN

Signature :

ABSTRACT

MATHEMATICAL MODELLING OF BLOOD FLOW THROUGH ARTERIES AND INVESTIGATION OF SOME PATHOLOGICAL CASES IN CARDIOVASCULAR SYSTEM USING GRAD-DIV STABILIZATION

Kökten, İsmail Tahir
M.S., Department of Mathematics
Supervisor: Prof. Dr. Songül Kaya Merdan

December 2019, 87 pages

In this thesis, we investigate the grad-div stabilization method and its feasibility on the cardiovascular system. Governing equations on blood flow is chosen to be Navier-Stokes and numerical solution is obtained by Galerkin finite element approximation. Grad-div stabilization is known as an effective residual based stabilization method and no study exists about its effect on the cardiovascular system. In this thesis, we present a grad-div stabilized fully discrete scheme with backward Euler time discretization, then present its stability and error analysis. To understand its effect on the cardiovascular system, we investigate some numerical cases such as stenosis, aneurysm and branching arteries by considering the changes in velocity, pressure and wall shear stress values. We also numerically investigate the pulsatile nature of blood flow and present some remarks on grad-div stabilization technique. With selection of a $O(1)$ stabilization parameter, the grad-div stabilization method validate the physical expectations in all the experiments, and contribute observable improvement in eccentric stenosis and rate of stenosis problems. We conclude that the grad-div stabilization method is efficient for the cardiovascular system and promising for future studies.

Keywords: Cardiovascular system, Navier-Stokes equations, backward Euler's method, error analysis, grad-div stabilization

ÖZ

ATARDAMARLARDAKİ KAN AKIŞININ GRAD-DİV KARARLILAŞTIRMA YÖNTEMİ KULLANILARAK MATEMATİKSEL MODELLENMESİ VE KARDİYOVASKÜLER SİSTEMDEKİ BAZI PATOLOJİK DURUMLARIN İNCELENMESİ

Kökten, İsmail Tahir
Yüksek Lisans, Matematik Bölümü
Tez Yöneticisi: Prof. Dr. Songül Kaya Merdan

Aralık 2019 , 87 sayfa

Bu tezde grad-div kararlılaştırma metodunu ve bu metodun kardiyovasküler sistem üzerindeki uygulanabilirliğini incelendik. Kan akışı üzerinde etkin olması için Navier-Stokes denklemleri seçildi ve nümerik çözümler Galerkin sonlu elemanlar yöntemi ile elde edildi. Grad-div metodu, etkili bir kalan tabanlı kararlılaştırma metodu olarak bilinmekte ve kardiyovasküler sistem üzerindeki etkisini inceleyen herhangi bir çalışma bulunmamaktadır. Biz bu tezde grad-div kararlılaştırmalı geri Euler metodu ile tam ayrık çözüm şeması, sonrasında da bunun kararlılık ve hata analizini sunduk. Kardiyovasküler sistem üzerindeki etkisini incelemek için, hız, basınç ve duvar kayma gerilimi değerlerini kullanarak stenoz, anevrizma ve arter dallanması durumlarını inceledik. Aynı zamanda kan akışının vurmalı yapısını da inceledik ve grad-div stabilizasyon yöntemi hakkında bazı sonuçları paylaştık. $O(1)$ olarak seçilen stabilizasyon parametresi için grad-div stabilizasyonunun tüm deneylerde fiziksel beklentileri karşıladığı, eksantrik stenoz ve stenoz oranı problemlerinde gözlemlenebilir katkı sağladığı görülmüştür. Grad-div stabilizasyon metodunun kardiyovasküler sistemin

incelenmesinde etkili olduğu ve ileriki çalışmalar için ümit verici olduğu sonucuna varılmıştır.

Anahtar Kelimeler: Kardiyovasküker sistem, Navier-Stokes denklemleri, geri Euler metodu, hata analizi, grad-div kararlılaştırma metodu

to my father and future children

ACKNOWLEDGMENTS

First things first, I would like to thank my advisor Prof. Songül KAYA MERDAN for her endless support. Her patience and guidance showed me path and motivated me to finish my thesis. I would also like to thank Assoc. Prof. Aytekin ÇIBIK for his insightful comments and contributions.

This is a humble thesis, indeed. Hope it may constitute a drop in the sea of science. METU have been the place that I healed from my physical problems, and breaked most of the molds in my mind which were mainly created by the society and the education system.

The first day I came to METU, I have seen Prof. Mustafa Hurşit ÖNSİPER, we had that nice conversation on foot at the corridors of our department. Observing my anxious state, he was telling me some advices. We have made many conversations for years, I am truely thank to him for his valuable contributions to my inner world and understanding of things. I will carry them until the last day of my life.

I would also like to thank my friend Duygu VARGÜN for her discussion on mathematical analysis sections and motivations in the process. Also many thanks to Dr. Hüseyin Enes SALMAN for his discussions on numerical results, and his endless support. I would like to thank Nuclear Medicine Physician Burcu DİRLİK SERİM, M.D. for her comments on the chapter about the cardiovascular system, helping me to question deeper on the concepts and have a more holistic understanding.

Lastly, I would like to send a couple notes to my future children. I have lost my father when I was 9, grew up with my elder brother and venerable mother. Long we have searched about our father, what he thinks about life and people. I would like to make this process easier for my children, in case they face similar situation.

My dear children, I have grown up with physical problems. It was 27 when I got free of them, now living more stable life with acceptance. I have a couple advices, hope they work for you. Please judge less, observe more. Not only the things and people, do it also for your thoughts, become observant on them. Be kind to yourself, so that

you will become kind to others. If you judge people, you will also judge yourself, this is why many people unhappy. If you prefer to judge, judge not with your EGO or emotions, but with your intellect and reasoning.

Learn that you shouldn't take things personal. Once you take some path understanding the mechanism behind human behaviours and cognitive processes, you will note that we all are the same, and all the behaviours comes from the similar mechanism. Read psychology and philosophy and ponder. Whatever you read or learn, know that you have the real book inside.

Please understand that we are not in this world to become rich or professors, those are only titles and things that society values and we follow unconsciously. Hope you have chance to escape from the rotten education system as fast as possible, join inside people, work early, sell something, talk with them. People are all mirror for us that we can see ourselves. If this mirror is blurred, please check your EGO. You may again join the education system for your graduate studies, but do it with awareness after you know yourself better.

While you chase things, please do not miss life. Focus on your physical sensations, try to live in the present moment. Meditations are great tool for that, you may meditate for sometime of your life. Note that we all have equal importance, but sticking some values you may be a valuable person. Please question your values, don't get obsessed with them, use them as benchmark to locate where you are, so that you can be on path as a human and free like an animal. Do not exaggerate your suffering, what ever you suffer, there are millions suffer even more.

Maybe some of them are wrong for you, but this is what life taught to me until my 30. Now I am searching for your mother, hope to meet with you very soon. Last words to you from Rumi;

I come to you without me, come to me without you.
Self is the thorn in the sole of the soul.
Merge with others,
If you stay in self, you are a grain, you are a drop,
If you merge with others, you are an ocean, you are a mine.

TABLE OF CONTENTS

LIST OF TABLES

TABLES

LIST OF FIGURES

FIGURES

CHAPTER 1

INTRODUCTION

The cardiovascular system circulates the blood and transport oxygen, nutrients, hormones, waste products and various chemicals around the body. While it acts as a transportation system, it also regulates pH, body temperature, hemostasis and work as a repair and immune system. Cardiovascular system involves three main components; heart, blood and the blood vessels. Blood is the fluid that contains materials to transport, blood vessels are the channels that carries blood and those materials to different body parts and the heart creates the pressure gradient to push the blood through the body.

Cardiovascular diseases can be defined as the dysfunctioning in heart, vessels and blood. Those cases involve narrowed, plugged, weakened or expanded vessels, heart failure and stroke. According to data from World Health Organization, cardiovascular diseases are the leading cause of death globally. 17.9 millon people die every year, which corresponds to 31 percent of all deaths worldwide and it is primarily caused by tobacco and harmful use of alcohol, sedentary life style and unhealthy eating habits [1].

While statistics on cardiovascular diseases clearly shows that it does really matter, a better understanding of cardiovascular system also matters. Mathematical models are useful to describe some cases in terms of mathematical concepts, while algorithms and simulations are useful to visualize these behaviors. Mathematical modeling and simulation of blood flow aims to understand the conditions that are effecting the functioning of cardiovascular system in different situations such as stenosis, atherosclerosis and other types of anomalies that occur in cardiovascular system. These applications are also useful to optimize surgical procedures and designing medical devices.

With advancement of more powerful computers, image processing and geometry extraction techniques, and studies to develop better algortihms, the demand for blood flow modeling is increased among researchers [2].

The most famous and accepted equation to model the blood flow is the Navier-Stokes equations, which were derived in 1820's by Navier and Stokes to describe how velocity, pressure and density of a fluid are connected. These equations are very hard to solve and admits very narrow range of analytic solutions. For complex domains, problem becomes harder to solve, however, with development of numerical algorithms and advancements in computer systems, we are now able to solve these equations in many complex domains and boundary conditions.

The most popular method to solve not only Navier-Stokes, but many other partial differential equations numerically is the finite element method, which involves separating the domain into elements and approximate the solution as a linear combination of basis functions on these elements. In this formulization, large variations in some fluid properties may cause some instabilities. The grad-div stabilization is one of the methods to prevent instabilities stemming from conservation of mass, by adding an extra penalty term in finite element formulization of Navier-Stokes equations [3].

Together with solutions of velocity, pressure fields and streamlines, we may also obtain wall shear stress by post processing the solution data, and those information gives a reasonably good clue to understand the blood flow phenomenon. A consistently low or oscillating shear stress proved to be signs of vessel anomalies due to constant damage on endothelial cells and it is really difficult to measure these values in a real patient, while modeling is really easier and can be integrated to diagnosis and prognosis process of patients [2, 4, 5].

This thesis has two main goals, first is to construct a numerically stable algorithm to solve Navier-Stokes equations together with grad-div stabilization. Another goal is to investigate how effective is the grad-div stabilization in cardiovascular system, since it has not been studied in this perspective in the literature yet. To investigate this properly, this thesis is organized as follows;

Chapter 2 : A brief introduction of cardiovascular system is presented to link the anatomy, physiology and pathology with mathematics and to get acquainted with

some important concepts so as to understand the phenomenon more holistically .

Chapter 3 : A brief introduction of mathematical aspects on cardiovascular system is presented to see the phenomenon in different perspectives, therefore one shall locate our study in whole frame.

Chapter 4 : Some inequalities, theorems and lemmas which are used in stability and error analysis of the proposed scheme are presented.

Chapter 5 : Navier-Stokes equations are presented and grad-div stabilized fully discrete scheme is obtained.

Chapter 6 : Stability and error analysis of proposed scheme is investigated.

Chapter 7 : The proposed method is used to numerically solve the equations and simulate some dysfunctionings in cardiovascular system, such as stenosis and aneurysm. Furthermore, the behavior of blood flow in arterial bifurcations presented and pulsatile nature of the blood flow is also investigated.

Chapter 8 : Some conclusions and remarks on grad-div stabilization and remarks on its feasibility in cardiovascular system are presented.

CHAPTER 2

CARDIOVASCULAR SYSTEM IN A NUTSHELL

In this chapter, we briefly introduce some concepts on cardiovascular system. Since we are interested in mathematics of the cardiovascular system, without giving much detail, we prefer to present a brief introduction to readers so as to introduce the whole system in a nutshell.

Anatomy, physiology and pathology are branches of biology and medicine. Anatomy refers to investigating structures of the living bodies; details about their structure, microstructure, sizes and locations, while physiology is interested in their functioning and the relationships between the components. Lastly, the dysfunctionings such as stenosis and aneurysm refer to the pathology of the cardiovascular system. Investigation of the cardiovascular system on these three branches are important to understand the mechanics behind it, and come up with more accurate models and solutions.

The cardiovascular system consists of three main components, the heart, vessels and the blood. Let us briefly introduce some main concepts and features.

2.1 Heart

The heart is a muscular organ, and its main goal is to pump the blood through the body and maintain the pressure gradient required to constantly circulate the blood through the circulatory system. The heart is located in the mediastinum area i.e. between two lungs, and most of its mass is generally at the left of the mid line [6]. It is also described in Figure 2.1 that the heart is encircled with two layered sac, the outer part is called the fibrous pericardium, protects the heart and prevents it from steep stretching and the inner part serous pericardium consists of parietal and visceral layers ,and there is a space called pericardial cavity between them, which contains

serous fluid that prevents friction during the heart beat.

Inside this sac, there is the heart wall consisting of three layers: epicardium; a thin

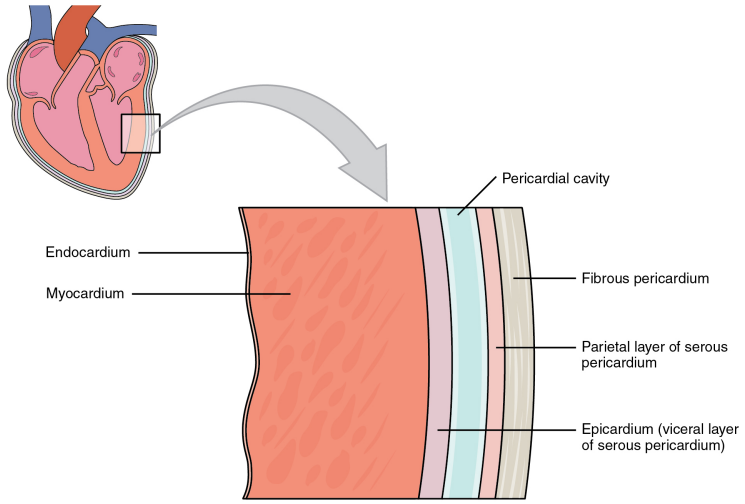

Figure 2.1: Image from [53], illustrates a cross-section of the heart. It is surrounded with a two layered sac, and there is a three layered wall beneath this sac; see also [2, 7].

layer that slicks and protects the heart, myocardium; the thick muscular layer containing cardiac muscles and endocardium; a thin layer consisting of endothelial cells, constitute the innermost surface of the heart [2, 7].

The heart is divided into two parts by the septum: right and left, and each part consists of ventricles and atrium. This division constitutes four chambers of the heart: the right ventricle (RV) and the left ventricle (LV) are the inferior chambers, which are high pressure points that the blood is released, and right atrium (RA) and left atrium (LA) are the low pressure points where the blood is received [2, 7]. Four chambers of the heart and their connecting vessels are decribed in Figure 2.2. The heart maintains this pressure gradient so that blood can move from the high pressure regions (ventricles) to the low pressure regions(atria). Ventricles have thick walls since they are high pressure points, and discharging of these chambers need more muscle activity [2, 8].

The heart is connected to the body with two types of vessels. With a couple exceptions, arteries carry the oxygenated blood away from the heart, and veins carry the deoxyganeted blood through the heart. Blood moving away from heart have two types of circulations: the first is the pulmonary circulation, which cleanses the blood in the lungs, and the second is the systemic circulation, which delivers the oxygenated blood through the body and gather waste products and deoxygenated blood into the

heart [2].

The pulmonary circulation starts from contraction of right ventricles and the opening

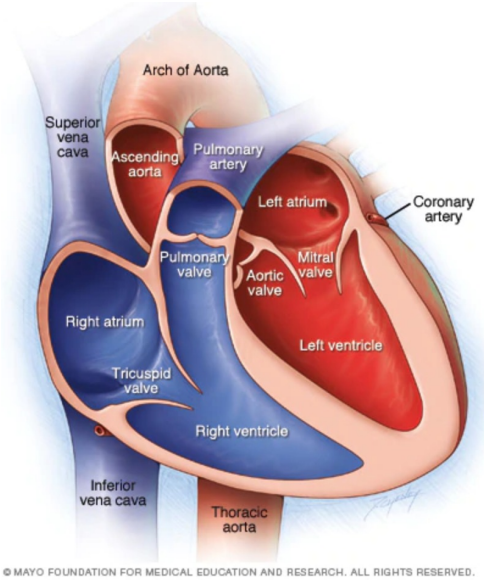

Figure 2.2: Image from [54], illustrates chambers and valves of the heart, together with the vessels connecting with body. The deoxygenated blood leaves the heart from the pulmonary artery to the lungs, while oxygenated blood leaves from the aorta to the body. Blood receives to the atria, and leaves the heart from the ventricles with a ventricular contraction; see also [2, 7].

of pulmonary valves. The blood discharges through pulmonary artery, deoxygenated blood gets oxygenated from the lungs. After that, the oxygenated blood arrives into low pressure point the LA through pulmonary veins. Finally, the blood moves to the LV through mitral valve by contraction of the LA. Secondly, the systemic circulation starts from contraction of the LV, the blood moves through aortic valves to the aorta. It moves all around the body and reaches to the low pressure area, RA through the superior and inferior venacava. After that, it moves to the RV through the tricuspid valve [2]. A sketch for two circulations is given in Figure 2.3.

In this process, valves (see the valves in Figure 2.2) helps the heart to maintain its high and low pressure in the chambers by preventing backflow during the transitions, therefore maintains the pressure gradient. The systole and the diastole are two important concepts to understand the pulsatile nature of the heart. When the pulmonary and aortic valves are close, and tricuspid valve and mitral valves are open, ventricles are relaxed and ready to receive blood. This relaxed state, resulting in ventricles filled with blood is called diastole. Once the mithral and tricuspid valves close,

ventricles are contracted to create pressure and pump the blood through the body, then pulmonary and the aortic valves open. This contracted state is called systole [2, 9, 10, 11]. Systole and diastole phases of the cardiac cycle is given in Figure 2.4.

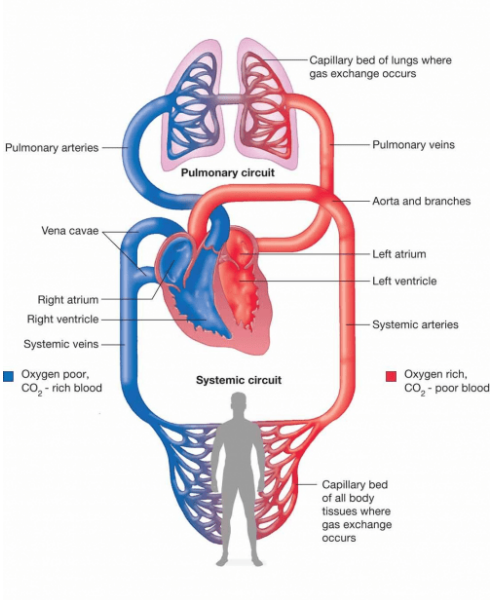

Figure 2.3: Image from [55], illustrates two types of circulations. The pulmonary circulation results with oxygenation of the blood through the lungs. In the systemic circulation, oxygen and various nutrients are delivered the body tissues and wastes are gathered from the body tissues. The red vessels indicate oxygenated blood and the blue vessels indicate deoxygenated blood; see also [2].

Understanding the blood pressure is important to investigate the mechanics of the cardiovascular system, especially the vascular system. The blood pressure is defined as the pressure made by the blood through the vessel walls. Measuring the blood pressure in the arteries when the ventricles are relax (diastole), we obtain diastolic blood pressure, and the peak pressure produced by contracted ventricles (systole) is called systolic blood pressure [2, 11].

The cardiac output, the heart rate and the stroke volume are three important concepts to understand the heart physiology and the heart mechanics. The heart rate is defined as the number of heart beats per minute, and the stroke volume is defined as the volume of the blood pumped by the heart per beat. Finally, the cardiac output is defined as the volume of the blood pumped by the heart in a time interval. The cardiac output is evaluated by the product of heart rate and the stroke volume [2, 12]. The cardiac output of a young adult is about 6 L/min with a heart rate of typically 1.25 Hz (75

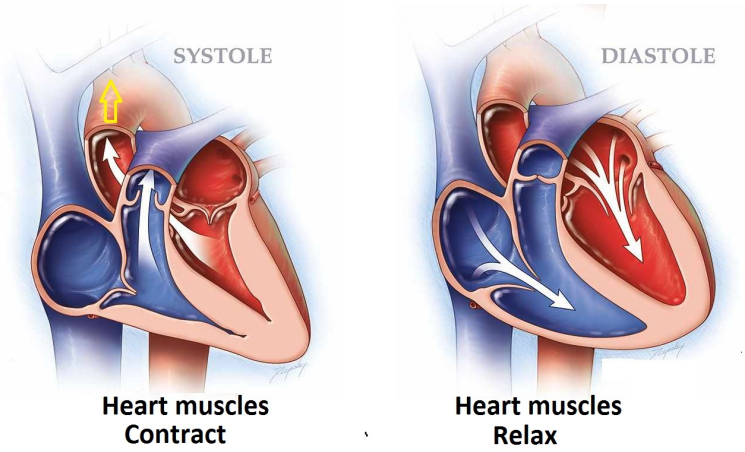

Figure 2.4: Image from [56], illustrates the diastole and the systole. The relaxed state of the ventricles is called diastole. In this phase, ventricles fills with blood. The contracted state of the ventricles is called systole. In systole, blood filled in the ventricles is pumped; see also [2, 11].

beats/min). The stroke volume of a young adult is typically 80 mL/beat, and abnormal measure of cardiac output can be an indication of a cardiovascular disease [2].

To beat the heart, it creates electrical impulses which are constantly generated peri-

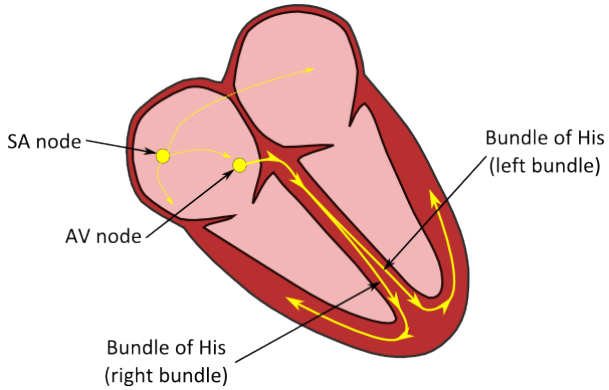

Figure 2.5: Image from [57], illustrates the elements of intrinsic cardiac conduction system. The pulse is generated at the SA nodes by pacemaker cells, then arrives to AV node. After a small delay it arrives to the ventricles through the bundle of his, and contracts the ventricles; see also [13].

odically by pacemaker cells, and heart rate is controlled by these impulses. The pacemaker cells are a type of cardiac myocytes that can make their own depolarization, while other cells need an initial stimulation for depolarization. Therefore pacemaker cells create the hearts intrinsic electrical activity, and this autonomous pacemaking process is the key to understand the pulsatile nature of the blood flow and the cardiac cycle. Sinoatrial node (SA node) and atrioventricular node (AV node) (highlighted in

Figure 2.5) in the heart contains pacemaker cells [13].

The cardiac cycle, detalied in Figure 2.6, starts with stimulus of the SA node, that

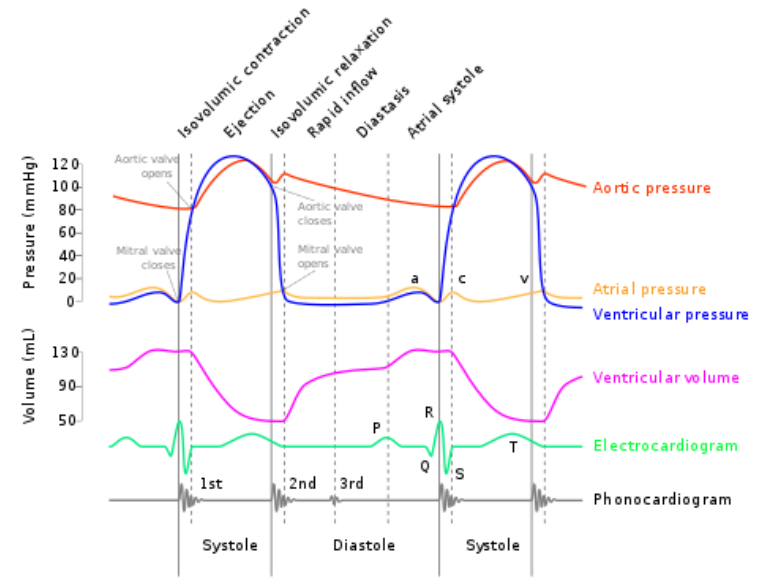

Figure 2.6: Image from [58], illustrates important variations during the cardiac cycle. At systole, ventricular and aortic pressure is increased with ventricular contraction, and ventricular volume is decreased with ejection. Diastole is the relaxed state of ventricles with low ventricular pressure. At diastole, ventricular volume increases and aortic pressure decreases. Electrocardiogram is mainly used to understand irregularities in the rhythm of the heart. With stimulation of SA node, atria are depolarized, therefore discharges the blood. This depolarization is shown in P wave. The delay in AV node is apparent between P wave and Q wave. The QRS wave represents the pulse that reaches from bundle of his and causes ventricular contraction. After a delay between ST segment, ventricles start to repolarize; see also [2, 8, 14].

starts the contraction of the atria (P wave on the electrocardiogram). Then the pressure in the atria increased, and the ventricles starts to fill. Once the phase starts to end, atrial contraction also ends. After that, the pressure at the atria starts to decrease, then the valves gets closed and contraction of ventricles starts to increase (QRS comlex), and the semilunar valves gets closed for some time. After the pressure increased enough to open the aortic and pulmonary valves, the blood is pushed from the heart (T wave). Together with the ejection, the pressure decreases and semilunar valve gets closed and one cardiac cycle ends [2, 8, 14].

2.2 Vessels

Vessels deliver oxygen and nutrients through the body, carry waste products and contributes to the blood pressure by dilation and contraction. Blood leaving the heart to deliver oxygen to a body part, leaves heart from an artery, then moves into smaller arteries called arterioles, and then capillaries to deliver oxygen and nutrients to the tissues. After that, the deoxygenated blood with waste products moves to the venules, which are small vein components takes the blood from capillaries, then to the veins and reaches to the heart from the superior and the inferior vena cava. The vessels and their connections are given in Figure 2.7. Since the pressure gradient between the ventricles and the capillaries is higher than the capillaries to the atrias, the veins have valves to prevent backflow of the blood in the veins [2].

Inside of a blood vessel, where the blood flows is called lumen and the blood vessels

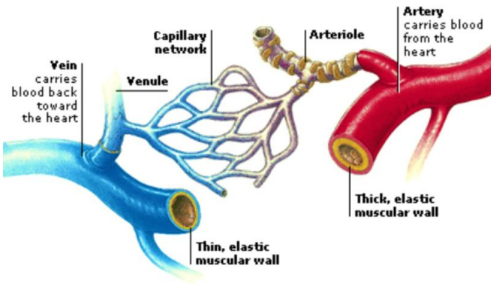

Figure 2.7: Image from [59], illustrates different types of vessels. Blood leaves heart through arteries, then moves through smaller branches of arteries called arterioles, then flows through very small vessels called capillaries for exchange of nutrients and waste products. Deoxygenated blood then moves through small vessels called venules. The blood then flows through larger vessels called veins, finally reaches to the heart; see also [2].

consists of three layers: Tunica adventitia constitutes the most outer layer and is made of collagen fibers, thus provides protection and resists agains the pressure. The tunica media constitutes the middle layer, made of smooth muscle cells and elastic fibers. It allows the vessels to dilate or constricts to adjust based on the blood volume needed to carry, and finally the tunica intima is the innermost layer, consists of endothelial cells that makes the first contact with the blood [2]. A detailed sketch is given in Figure 2.8 to compare the wall anatomy of artery and veins. To understand the variability of vessels in number, size and pressure, some features of important vessels are given in Table 2.1 and 2.2

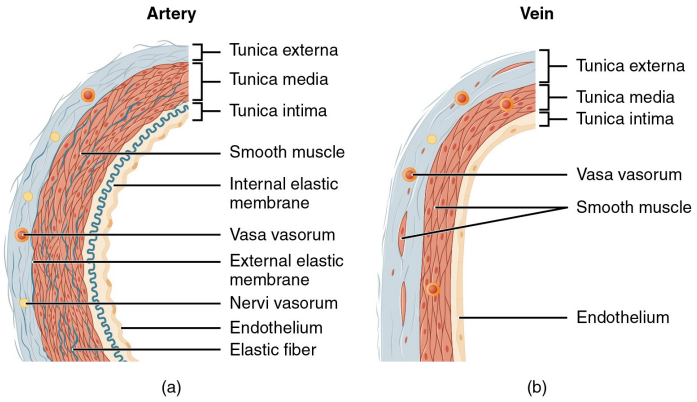

Figure 2.8: Image from part of [60], illustrates anatomy of arteries and veins. In both types of vessels, the outer layer provides protection, the middle layer contain muscles, and provides mobility, while the innermost layer provides the contact and the exchange with the blood. Since arteries are closer to the heart and imposed to greater pressure and need more elasticity, they have a thicker wall. Veins have smaller lumen since they move from a smaller pressure gradient; see also [2].

Table 2.1: Some properties of systemic vessels are introduced. Adapted from [2], p. 6.

Vessel	Diameter of Lumen(mm)	Wall Thickness(mm)	Mean Pressure(kPa)	Number of Vessels
Aorta	25	2	12.5	1
Large Arteries	1-10	1	12	50
Small Arteries	.5-1	1	12	10^3
Arteriole	.01 - .5	0.03	7	10^4
Capillary	.006-.01	0.001	3	10^6
Venule	.01-.5	0.003	1.5	10^4
Vein	.5-15	0.5	1	10^3
Vena cava	30	1.5	0.5	2

The endothelial cells are one of the basic components of the cardiovascular system. They are small and stand between the blood and the vessel wall as endothelium layer, it basically turns shear stress from blood into biochemical signals [2, 15]. The endothelial cells are exposed to shear stress due to friction of the blood, and normal stress due to blood pressure. It takes action on the control of the exchange between blood and the vessel wall and immune responses. Wall shear stress is one important feature to study the effects of fluid forces into the endothelial cells, on drug secretion

Table 2.2: Some properties of pulmonary vessels are introduced. Adapted from [2], p. 6.

Diameter of Lumen(mm)	Number of Vessels	Mean Velocity(mm/s)
30	1	110
8-30	10	155
1-8	10^3	104
0.1 - 1	0.25×10^6	44
0.02-0.1	0.20×10^6	23
0.01	300×10^6	2

or deterring adhesiveness of the wall and some complications such as extravasation [2].

A very important molecule that takes place on adhesiveness and dilation of vessel is nitric oxide (NO). It is released by endothelial cells to arrange contraction of vessels, it also decreases platelet aggregation. Endothelial cells sense increased blood pressure by shear stress, and trigger NO production. NO relaxes the smooth muscle cells and dilates the vessel to regulate the blood pressure as a local response for high blood pressure and high shear stress. A dysfunction in endothelial layer and deterioration on endothelium line-up effects discharging of NO, and cause aggregation of materials into vessel wall, therefore causes narrowing of blood vessel [2].

Depending on the flow over the vessel, shape of endothelial cells may be circular (low flow) and wider for high and undirectional flow. They change their orientation depending on magnitude and direction of the flow. It is also very important for investigation of the vascular pathology, e.g. possibility of atherosclerosis formation increases as endothelial cells fail to align in the flow direction, while this situation is caused by oscillating or low shear stress [15, 2].

Depending on the changes in blood pressure, shear stress and tension, vessels rebuild the accustomed condition either applying some changes in the whole cardiovascular system or remodelling their wall. Since wall shear stress is related with accumu-

lated fatty deposits, it is one of the first things to investigate for such changes. Also due to the pulsatile nature of the blood flow, wall shear stress values experience high fluctuations. Also due to wobbly nature of pressure pulses and anisotropic structure of vessel walls and complicated geometries such as branching vessels, high pressure fluctuations occurs and this may lead some complications, and cardiovascular system has some natural response for that [2].

Vessels responds to increased pressure and flow by increasing its diameter, and de-

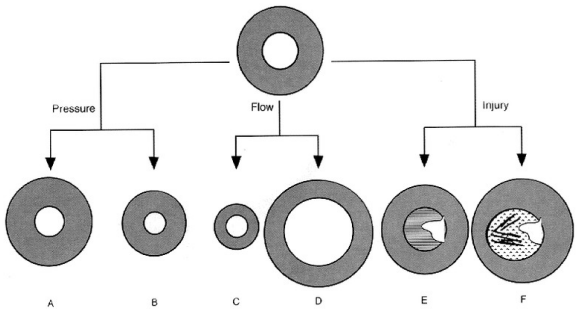

Figure 2.9: Image from [61], illustrates patterns in vessel wall remodelling. Classification of vessel wall remodelling is based on the blood pressure, the flow patterns and anomalies on the vessel. Remodelling on vessel wall are expressed in terms of media to lumen ratio (M/L). A shows an increased ratio while B shows a decreased ratio. C and D happens due to flow patterns, D maybe caused by some anomalies such as arteriovenous fistula or cellular loss and may cause development of an aneurysm, while C leads a continued low blood flow. E and F may be caused by a abnormal response to a vascular injury; see also [2, 16].

creased pressure and flow by decreasing the diameter. High blood pressure leads thickened arterial walls of the vessel, as an adverse affect of these pressure changes. Also an increased wall shear stress triggers restructuring of the vessel walls [2]. Some remodeling patterns are given in Figure 2.9.

2.3 Blood

Blood is a very important liquid, it helps to maintain and regulate body temperature, pH levels. It contributes to the protection from infections, and repair of the body. Understanding the structure and the ingredients of the blood is important for accurate modeling of blood flow phenomena. Blood consists 45 % of red blood cells and 55 %

of plasma. The plasma is approximately 92 % of water, the remaining is electrolytes, hormones, proteins, gases and waste products. This suspending nature of the blood forces us to choose between Newtonian and non-Newtonian models, depending on the vessel geometry that we are studying on. Blood for a healthy person is given in Table 2.3.

Table 2.3: Some properties for blood for a healthy person are introduced. Adapted from [2], p. 23.

Density	Viscosity	Mean Velocity(mm/s)
Viscosity	1	64
Osmotic Pressure	10	21
pH	10^3	37
0.1 - 1	0.25×10^6	19
0.02-0.1	0.20×10^6	5
0.01	300×10^6	5

2.4 Cardiovascular Diseases

Dysfunctions (morphological changes on vessels, vessels walls or mechanical changes such as hypertension) on cardiovascular system are called cardiovascular diseases. Heart attack, heart failure, heart valve disease, heart muscle disease (cardiomyopathy) and vascular diseases are some important cardiovascular diseases and they are the number one cause of death worldwide [2]. Atherosclerosis and aneurysm are two of the most common vascular diseases and many studies on the literature exists on those problems.

2.4.1 Atherosclerosis

Arteries are blood vessels that generally carry oxygen-rich blood from the heart to other parts of the body. Plaque builts inside arteries are called Atherosclerosis. Fat, cholesterol, calcium or other substances may cause plaque development. A plaque develops in decades, the early stages of this development is benign. However, it should invade the vessel lumen and disturb the blood flow as it gets bigger. Development of a thrombi or a rupture is more dangerous and unwanted scenario; it may cause stroke,

heart attack or more serious problems. Together they comprise approximately half of all the deaths in developed countries[17]. Development stages of an atherosclerosis is given in Figure 2.10

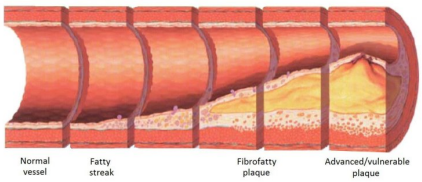

Figure 2.10: Image from [62], illustrates the progression of atherosclerosis and endothelial dysfunction, mainly due to accumulation of lipids; see also [18].

2.4.2 Aneurysm

Dilation of a vessel and as a baloon like shape over years is called aneurysm. Aneurysm occurs due to weakening of vessel walls as well as some other diseases. There are two types of aneurysm: saccular and fusiform (see Figure 2.11). If whole vessel circumference is weakened and dilation becomes at all sides, it is called fusiform aneurysm. If only one side of a vessel is weakened and the dilation becomes into one side, it is called saccular aneurysm. Its rupture may lead to haemorrhage, while a rupture in the brain may lead to lethal vasospasm [2].

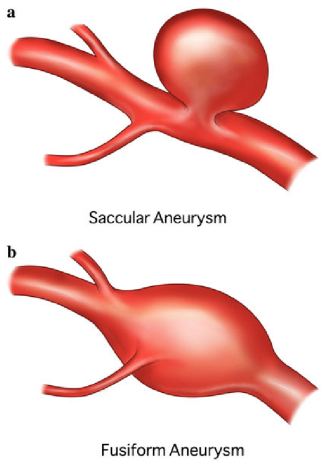

Figure 2.11: Image from [63], illustrates two kinds of aneurysm. In saccular aneurysm, local dilation occurs and the deformed vessel takes a saccular shape. In fusiform aneurysm, vessel takes a balloon like shape, and dilation occurs from all sides of vessel; see also [2].

CHAPTER 3

MATHEMATICS OF CARDIOVASCULAR SYSTEM

In this section, we will introduce some mathematical aspects and motivations on cardiovascular system. In general, modeling of any phenomena comes from an observed problem. To understand the problem, a mathematical model needs to be established, which involves defining appropriate geometry, picking appropriate equations, applying suitable numerical methods and simulating the results in order to compare them with actual experimental data [23].

When we compare with actual experimental data in modeling of cardiovascular system, there are two types of data: in vivo, which is taken from real patients, more reliable but costly and time consuming, and in vitro, which is generated from a controlled environment which is less precise but less costly and time saving. Using any of those types, a researcher can understand whether the model is reliable, otherwise it needs to be pivoted [2].

Before we start mathematical modeling of a phenomenon, we need to establish the geometry where the equations going to be solved. One possible way is to draw it manually, where as with development of image segmentation techniques it is possible to extract a realistic and proper geometry from medical images such as CT and MRI. The extracted edge map is smoothed and reconstructed with interpolation, and developing robust algortihms to obtain sufficiently smooth shapes with as less user interaction as possible is another concern of the literature [2, 19].

From specific to more general, investigation of fluid in single artery is called local flow analysis, while investigation of the interaction of fluid and the arterial deformation is called fluid-structure interaction. Understanding the behavior of whole system from modeling of single artery is called geometric multiscale modeling, and under-

standing of a global scenario is the desired aim of mathematical modeling [23, 20].

Talking on a local level, before modeling of a single artery representation of fluid field is important. At one side Lagrangian representation aims to follow single fluid particle which is not appropriate due to complex pattern of cardiovascular system. On the other side, Eulerian approach aims to investigate behavior of fluid particles in a specific part of an artery, which miss the deformation of an artery. One very common approach is the Arbitrary Lagrangian-Eulerian (ALE) approach which fixes inlet and outlet of a specific domain of the artery and allow the walls to deform, by combining both of the representations [2].

Blood is a suspending plasma mainly consisting of water, and includes blood cells inside. One apparent effect of this is so-called share-thinning, which can be described as the behavior of fluids, whose viscosity decreases under shear strain (see Figure 3.1). That is to say, with increased rate of deformation, a shear-thinning fluid becomes more fluent. With decreasing vessel diameter, shear-thinning effect increases [2]. Shear-thinning is essential for blood to perfuse into the body, and red blood cells are the most important component of blood that is related to shear-thinning property of blood [21, 22].

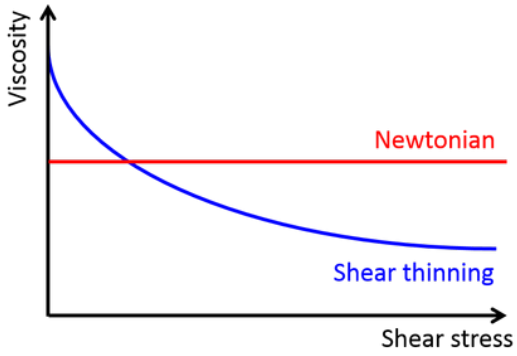

Figure 3.1: Image from [64], illustrates the effect of shear stress on viscosity; see also [2].

For vessels that has diameter of less than about $1mm$, viscosity of the blood decreases and becomes dependent on the vessel diameter. In such small vessels, plasma contacts with vessel wall, and erythrocytes moves from center of the vessel easily. Therefore viscosity decreases abruptly, this is known as Fahraeus-Lindqvist effect.
What's more, erythrocytes should be bigger than the smallest capillaries. At that

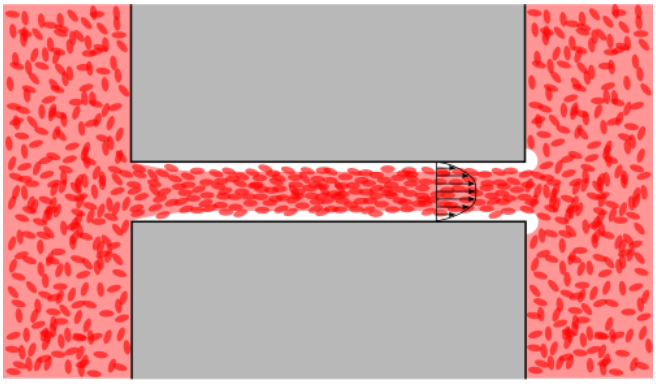

Figure 3.2: Image from [65], illustrates Fahraeus-Lindqvist effect stating the accumulation of red blood cells into the center of the vessel; see also [2].

point, erythrocytes goes under deformation, which is another viscoelastic behaviour of the blood that needs to be investigated. In that case the blood may not be treated as a continuous fluid. Understanding these properties, we can split mathematical models of blood flow as: Newtonian models, neglecting shear-thinning and viscoelastic effects, applicable in large vessels, and non-Newtonian models, viscoelastic effects are taken into account and is appropriate for vessels of diameter less than $1mm$. Since non-Newtonian behavior makes the viscosity dependent on shear rate, it increases the computational cost. Newtonian models usually used for the sake of simplicity [2].

The incompressible Navier-Stokes equations which governs the flow of blood is given by

$$\begin{aligned} u_t + (u \cdot \nabla)u - \nu \Delta u + \nabla p = f, \quad in \quad (0,T] \times \Omega \\ \nabla \cdot u = 0 \quad (0,T] \times \Omega \\ u(x,0) = u_0(x) \quad for \quad x \in \Omega \\ u = 0 \quad on \quad \Gamma_{Wall} \\ n \cdot \sigma = 0 \quad on \quad \Gamma_{out} \\ u = c \quad on \quad \Gamma_{in} \end{aligned} \tag{3.1}$$

Given a vessel domain Ω, the inlet Γ_{in} is called a proximal boundary since it is close to heart and the outlet Γ_{out} is called a distal boundary since it is farther from the heart. Γ_{Wall} are assumed to be fixed with no-slip boundary condition and normal

stress $\sigma \cdot n$ at distal boundaries [2]. The initial condition of velocity needs to be determined wisely, since $\nabla \cdot u_0 = 0$ needs to be satisfied. A very common approach to decrease the effect of wrong initial data is to solve stationary Stokes problem, and use the solutions as initial condition in Navier-Stokes equations[2].

The convective term $(u \cdot \nabla)u$ in Navier-Stokes equations (3.1) may cause instabilities such as turbulence, which may occur in CVS in small scales. Reynolds number (Re) is very important for flow characteristics: a flow with $Re < 1000$ is to remain stable and is called laminar flow regime where as higher Reynolds numbers may cause turbulence. Reynolds number in different vessels is given in Table 3.1 to understand the scale of Reynolds number in the cardiovascular system more clearly.

Table 3.1: Reynolds numbers for different vessels are introduced. Adapted from [2], p. 31.

Vessel	Reynolds Number (Re)
Ascending aorta	4000
Thoracic aorta	2500
Brachial artery	1000
Common carotid artery	800
LAD coronary artery	400
Small artery	100
Capillary	0.003
Large vein	1700

Even though, some instabilities at systolic phase may occur at the exit of the aorta, a full scale turbulence does not occur in the cardiovascular system [23]. Other possible cases of turbulence shall be increased heart rate, existence of stenosis, implant, aneurysm, branching arteries and decreased viscosity in special conditions such as anemia.

Another important calculation in CVS is wall shear stress (WSS), which corresponds to force per unit area caused by the friction of the blood into the vessel wall or tangential component of the stress on endothelial surface. It is well known that WSS and atherosclerosis formation has a significant relationship [4]. Low and oscillating WSS regions are to be susceptible places for plaque formation, due to alteration in

endothelium and aggregation of blood cells [2, 24]. Besides, on the stenosis region, large spatial WSS values together with fluctiating pressure is known to weaken the stenosis and may cause a rupture of the plaque [25].

Navier-Stokes equations involves information about pressure and velocity and allows us to compute in vitro shear stress values with some post processing. 0.5 to $1.2Pa$ of WSS values are acknowledged as normal, while values out of this range are regarded as low and high wall shear stress values. In case of pulsatile flow in straight geometry with laminar flow regime, WSS values changes between $1.7 - 7Pa$ [24]. Pulsatility

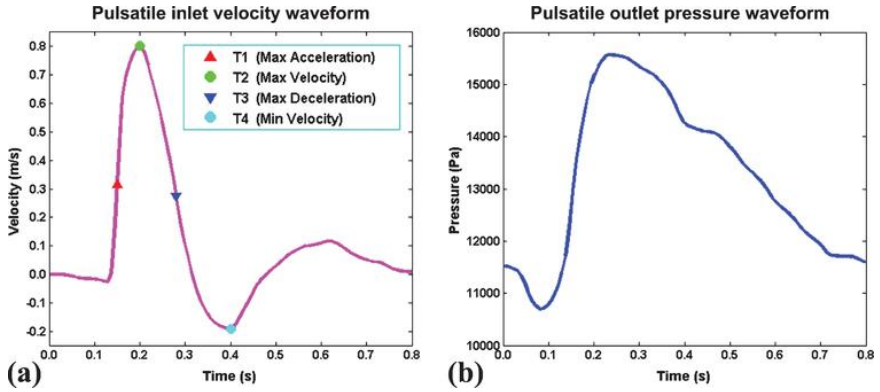

Figure 3.3: Image from [66], illustrates the inlet velocity profile and the outlet pressure profile.

of blood flow may promote plaque formation by causing reverse flow, and recirculations adversely affects the endothelium. Even though we use a periodic boundary condition to represent pulsatile nature of blood flow, this choice is not true in general. In Figure 3.3, the centerline velocity in a cardiac cycle is given to express pulsatile nature more clearly for different phases of contractions of the heart. With different physical activities, metabolic disorders, vasoconstriction or vasocontraction may occur and amount of blood sending different organs or heart rythm may change, which is a different area of research. Neglecting the pulsatile nature in peripheral arteries, veins and the capillary bed is somewhat reasonable since pulsatility of the flow is reduced due to regularity effects [2].

Local changes in body temperature may also effect flow patterns. In large and medium vessels, the effects should be less but in smaller vessels blood viscosity may be effected by temperature changes. Normally describing temperature change require another PDE coupled with NSE [2].

Throughout the thesis, we assume that, the blood is a homogeneous fluid. It is Newtonian with constant viscosity $0.0035 Pa{\cdot}s$ and vessel radius are selected large enough to make Newtonian flow justifiable. Also, blood density is chosen constant with $1060 \frac{kg}{m^3}$ with a constant temperature of general body temperature.

CHAPTER 4

MATHEMATICAL PRELIMINARIES

In this chapter, we will discuss some important definitions, lemmas and theorems that are used in mathematical analysis (Chapter 6) of this thesis. We have used mostly the references from [3, 26, 27, 28].

Definition 4.0.1 *(Hilbert Spaces) A complete normed vector space is called a Banach space and is called a Hilbert space if it is equipped with inner product.*

Remark 4.0.1 *In finite element approximation, we aim to find an approximate solution. Completeness of Hilbert space guarantees that the approximation will converge to a constructed sequence.*

We will now define the most important and commonly used Hilbert and Banach spaces consisting of functions and some special cases of these function spaces.

Definition 4.0.2 *(Lebesgue Spaces ($L^p(\Omega)$)) Let $\Omega \subset \mathbb{R}^n$, defining the norms*

$$\|v\|_{L^p(\Omega)} = \left(\int_\Omega |v|^p dx \right)^{\frac{1}{p}}, \quad 1 \leq p < \infty$$

and

$$\|v\|_{L^\infty(\Omega)} = \sup_{x \in \Omega} |v(x)|, \quad p = \infty$$

then $L^p(\Omega)$ function space is described as

$$L^p(\Omega) = \left\{ v : \Omega \to \mathbb{R} : \|v\|_{L^p(\Omega)} < \infty \right\}.$$

We have the only Hilbert space $L^2(\Omega)$, since we have $(u, v)_{L^2(\Omega)} = \int_\Omega uv dx$ is the inner product in this space. For other cases, $L^p(\Omega)$ spaces are Banach spaces.

Definition 4.0.3 *Let multi-index $\alpha = (\alpha_1, \alpha_2, ..., \alpha_d)$ be d-tuple of non-negative integers α_i. The order of α is defined by*

$$|\alpha| = \sum_{i=1}^{d} \alpha_i$$

and the classical partial derivative is defined by

$$D^{\alpha} = \prod_{i=1}^{|\alpha|} \left(\frac{\partial}{\partial x_i} \right)^{\alpha_i}.$$

Definition 4.0.4 *(Weak Derivative) Let the space of locally integrable functions be*

$$L^1_{loc}(\Omega) = \{v : v \in L^1(K), \forall K \subset\subset \Omega\}$$

for $u \in L^1_{loc}(\Omega)$ and ϕ be an infinitely differentiable compactly supported function, if there is a function $g \in L^1_{loc}(\Omega)$ such that,

$$\int_{\Omega} g\phi dx = (-1)^{|\alpha|} \int_{\Omega} uD^{\alpha}\phi dx,$$

then we call g as weak derivative D^{α} of u.

Definition 4.0.5 *(Sobolev Spaces) Assuming all the weak derivatives D^{α} of $u \in L^p(\Omega)$ exists, then the Sobolev space $W^p_k(\Omega)$ is defined by*

$$W^p_k(\Omega) = \left\{ u \in L^p(\Omega) : D^{\alpha}u \in L^p(\Omega), |\alpha| \leq k \right\}$$

with the norms

$$\|u\|_{W^p_k(\Omega)} = \left(\sum_{|\alpha| \leq k} \|D^{\alpha}u\|^p_{L^p(\Omega)} \right)^{\frac{1}{p}}, 1 \leq p < \infty$$

and

$$\|u\|_{W^p_k(\Omega)} = \max_{|\alpha| \leq k} \|D^{\alpha}u\|_{L^{\infty}(\Omega)}, p = \infty.$$

Remark 4.0.2 *One of the mostly used Sobolev space is W^2_k which is a Hilbert space. $H^k(\Omega) = W^2_k(\Omega)$ is to be used to show the relationship. We shall define*

$$H^1(\Omega) = W^2_1(\Omega) = \{u \in L^2(\Omega) : D^1u \in L^2(\Omega)\}$$

using the norm

$$\|u\|^2_{H^1(\Omega)} = \|u\|^2_{L^2(\Omega)} + \|\nabla u\|^2_{L^2(\Omega)}$$

and the inner product

$$(u,v)^2_{H^1(\Omega)} = (u,v)_{L^2(\Omega)} + (\nabla u, \nabla v)_{L^2(\Omega)}.$$

Definition 4.0.6 *The constrained Hilbert space H^1_0 can be defined as,*

$$H^1_0(\Omega) = \{u \in H^1(\Omega) : v|_{\partial\Omega} = 0\}.$$

Definition 4.0.7 *(Dual Norm) The norm of the dual space H^{-1} of H^1_0 is denoted by $||\cdot||_{-1}$. For $f \in L^2(\Omega)$, the dual norm of f is defined by,*

$$\|f\|_{-1} = \sup_{v \in H^1_0} \frac{(f,v)}{\|\nabla v\|}$$

Lemma 4.0.1 *(Ladyzhenskaya inequality) For a vector function $u : \mathbb{R}^d \longrightarrow \mathbb{R}^d$ with compact support and the indicated L^p norms finite, the following inequalities hold;*

$$||u||_{L^4(\mathbb{R}^2)} \leq 2^{\frac{1}{4}} ||u||^{\frac{1}{2}}_{L^2(\mathbb{R}^2)} ||\nabla u||^{\frac{1}{2}}_{L^2(\mathbb{R}^2)}$$

$$||u||_{L^4(R^3)} \leq \frac{4}{3\sqrt{3}} ||u||^{\frac{1}{4}} ||\nabla u||^{\frac{3}{4}}, (d=3)$$

Lemma 4.0.2 *(Poincaré-Friedrichs inequality) Let Ω a bounded set. As $v \in H^1_0(\Omega)$*

$$||v||_{L^2(\Omega)} \leq C||\nabla v||_{L^2(\Omega)}$$

for a positive constant C independent of v.

Theorem 4.0.1 *(Hölder's inequality) Let $f \in L^p(\Omega)$ and $g \in L^q(\Omega)$ with $\frac{1}{p} + \frac{1}{q} = 1$ where $p, q \in [0, \infty)$. Then*

$$\|fg\|_{L^1(\Omega)} \leq \|f\|_{L^p(\Omega)} \|g\|_{L^q(\Omega)}.$$

Remark 4.0.3 *Setting p=q=2 in Hölder's inequality gives the Cauchy-Schwarz inequality,*

$$\|fg\|_{L^1(\Omega)} \leq \|f\|_{L^2(\Omega)} \|g\|_{L^2(\Omega)}.$$

Definition 4.0.8 *(Young's inequality) For* $a, b, \epsilon > 0$ *and* $\frac{1}{p} + \frac{1}{q} = 1, 1 < p, q < \infty$*, the inequality*

$$ab \leq \frac{\epsilon}{p} a^p + \frac{\epsilon^{\frac{-p}{q}}}{q} a^q$$

holds.

Lemma 4.0.3 *For any* $v \in H^1(\Omega)$*, the following inequality holds*

$$\|\nabla \cdot v\| \leq \sqrt{d} \|\nabla v\|$$

Definition 4.0.9 *The space* $L^p(0, T; W_q^k(\Omega))$ *can be defined by;*

$$L^p(0, T; W_q^k(\Omega)) = \{\phi : (0, T) \to W_p^k(\Omega), \|\phi\|^2_{L^q(0,T;W_p^k(\Omega))} \leq \infty\}$$

for $\phi(x, t)$*, with the norm*

$$\|\phi\|_{L^q(0,T;W_p^k(\Omega))} = (\int_0^T \|\phi(t)\|^q_{W_p^k(\Omega)} dt)^{\frac{1}{q}}.$$

Lemma 4.0.4 *(Discrete Gronwall inequality) For* $n \geq 0$ *and non-negative integers* $a_N, b_n, c_n, d_n, \alpha_n$*, if*

$$a_{N+1} + \Delta t \sum_{n=1}^{N+1} b_n \leq \Delta t \sum_{n=1}^{N+1} \alpha_n d_n + \Delta t \sum_{n=1}^{N+1} c_n + B \quad N \geq 0,$$

holds, then

$$a_N + \Delta t \sum_{n=1}^{N+1} b_n \leq exp\left(\Delta t \sum_{n=1}^{N+1} \frac{\alpha_n}{1 - k\alpha_n}\right)\left(\Delta t \sum_{n=1}^{N+1} c_n + B\right) \quad N \geq 0,$$

for $k\alpha_n < 1$.

CHAPTER 5

NAVIER-STOKES EQUATIONS

Navier-Stokes equations are the most famous and accepted equation to model the fluid flow, stem from Newton's second law of motion and are widely used to describe motion of blood. It combines the concepts of velocity, momentum and conservation of mass, for some given initial conditions [3]. It is derived in 1820's by Navier and Stokes to describe how velocity, pressure and density of a fluid are connected. Unfortunately, Navier-Stokes equations are hard to solve and admits limited number of analytic solutions, and it gets harder for complex domains. Fortunately, with advancements in computer systems and development of numerical algorithms, it is solvable in many complex domains with more complicated boundary conditions.

Finite difference method (FDM), finite volume method (FVM) and Finite element method (FEM) are three popular methods to numerically solve partial differential equations. In solution of Navier-Stokes equations, FDM and FVM are used to approximate the so-called strong form of the Navier-Stokes equations with an easy implementation. However, they do not yield good results in curved boundaries and admits difficult convergence analysis. The most popular method is the FEM, approximates the so-called weak form of the Navier-Stokes equations, therefore it requires less assumptions on the domain and boundary conditions, and admits a greater range of approximate solutions [29, 30].

In this chapter, we first introduce the Navier-Stokes equations, which govern the blood motion. After that we obtain weak formulization of Navier-Stokes equations, then we introduce FEM to numerically solve them. We finally present the grad-div stabilized FEM formulation of Navier-Stokes equations. [31] by J. Donea and [3] by V. John are commonly used for the organization of this chapter.

Let $\Omega \subset \mathbb{R}^d$, $d = \{2, 3\}$ and the domain is bounded and the boundary $\Gamma = \partial\Omega$ is Lipschitz continuous. Then the time dependent Navier-Stokes equations are given by

$$\rho(u_t + (u \cdot \nabla)u) = \nabla \cdot \sigma + \rho f \quad in \quad (0, T] \times \Omega \tag{5.1}$$
$$\nabla \cdot u = 0 \quad (0, T] \times \Omega$$

here u is the velocity, ρ is the fluid density, f is the body force per unit mass of fluid and σ is the Cauchy stress tensor.

Before we decompose the Cauchy stress tensor, let us start by defining velocity gradient which describes how magnitude of velocity $v = (v_1, v_2, v_3)^T$ changes with distance $x = (x_1, x_2, x_3)^T$ and therefore cause a rotation or deformation on a single fluid particle,

$$\nabla v = \begin{pmatrix} \frac{\partial v_1}{\partial x_1} & \frac{\partial v_1}{\partial x_2} & \frac{\partial v_1}{\partial x_3} \\ \frac{\partial v_2}{\partial x_1} & \frac{\partial v_2}{\partial x_2} & \frac{\partial v_2}{\partial x_3} \\ \frac{\partial v_3}{\partial x_1} & \frac{\partial v_3}{\partial x_2} & \frac{\partial v_3}{\partial x_3} \end{pmatrix} \tag{5.2}$$

It can be decomposed into symetric and skew-symetric parts

$$\nabla^S := \frac{1}{2}(\nabla v + \nabla v^T) \tag{5.3}$$

$$\nabla^W := \frac{1}{2}(\nabla v - \nabla v^T)$$

where ∇^S is called the rate of deformation or velocity deformation tensor (strain rate) of the fluid and ∇^W is called vorticity (spin) tensor which describes local spinning motion of fluid particles.

If the fluid is not moving, then only normal forces of stress exists and it can be stated as $\sigma_{ij} = -p\delta_{ij}$ where δ_{ij} is the Kronecker delta and p is the fluid pressure at rest. If it is not at rest, then tangential stresses becomes nonzero, in this case the Cauchy stress tensor is stated as $\sigma_{ij} = -p\delta_{ij} + s_{i,j}$ where $s_{i,j}$ is called the deviatoric stress tensor.

If the fluid of interest is Newtonian, the stress tensor and rate of deformation tensor (symmetric part of velocity gradient) assumed to be linearly related with the equation

$$\sigma_{ij} = -p\delta_{ij} + \mu\left(\frac{\partial v_i}{\partial x_j} + \frac{\partial v_j}{\partial x_i}\right) + \lambda\frac{\partial v_k}{\partial x_k}\delta_{ij} \tag{5.4}$$

μ is the dynamic viscosity and $\mu\left(\frac{\partial v_i}{\partial x_j}+\frac{\partial v_j}{\partial x_i}\right)$ is the shear stress i.e. tangential component of stress tensor. Evaluation of this relation at wall, one shall obtain the wall shear stress, which has too many application on physics, and its applications on the cardiovascular system is mentioned in Chapter 4, and we will use this formula for the numerical simulations in Chapter 7.

Using $\nabla \cdot v = 0$, we obtain

$$\sigma_{ij} = -pI + 2\mu\nabla^S v \tag{5.5}$$

$$\begin{aligned} \begin{pmatrix} \sigma_{11} & \sigma_{12} & \sigma_{13} \\ \sigma_{21} & \sigma_{22} & \sigma_{23} \\ \sigma_{31} & \sigma_{32} & \sigma_{33} \end{pmatrix} &= -p \begin{pmatrix} 1 & 0 & 0 \\ 0 & 1 & 0 \\ 0 & 0 & 1 \end{pmatrix} \\ + \begin{pmatrix} \frac{\partial v_1}{\partial x_1} & \frac{1}{2}\left(\frac{\partial v_1}{\partial x_2}+\frac{\partial v_2}{\partial x_1}\right) & \frac{1}{2}\left(\frac{\partial v_1}{\partial x_3}+\frac{\partial v_3}{\partial x_1}\right) \\ \frac{1}{2}\left(\frac{\partial v_2}{\partial x_1}+\frac{\partial v_1}{\partial x_2}\right) & \frac{\partial v_2}{\partial x_2} & \frac{1}{2}\left(\frac{\partial v_2}{\partial x_3}+\frac{\partial v_3}{\partial x_2}\right) \\ \frac{1}{2}\left(\frac{\partial v_3}{\partial x_1}+\frac{\partial v_1}{\partial x_3}\right) & \frac{1}{2}\left(\frac{\partial v_3}{\partial x_2}+\frac{\partial v_2}{\partial x_3}\right) & \frac{\partial v_3}{\partial x_3} \end{pmatrix} \end{aligned} \tag{5.6}$$

Here, using the equation (5.5) for σ in equation (5.1), dividing both sides to ρ and substituting $\nu = \frac{\mu}{\rho}$, we have the Navier-Stokes equations

$$u_t + (u\cdot\nabla)u - 2\nu\nabla\cdot\nabla^S v + \nabla p = f \quad in \quad (0,T]\times\Omega \tag{5.7}$$

$$\nabla\cdot u = 0 \quad (0,T]\times\Omega$$

Here, $\nu = \frac{\mu}{\rho}$ is the fluid kinematic viscosity and p is the kinematic pressure. The term $u_t + (u\cdot\nabla)u$ here represents the inertial (momentum) forces, $\nu\nabla\cdot\nabla^s u$ represents the viscous forces, ∇p represents the pressure forces and f represents the external forces which is applied on fluid particles.

Substituting $\nabla^S u$ and rewritting it as

$$u_t + (u\cdot\nabla)u - \nu\nabla^2 u - \nu\nabla(\nabla\cdot u) + \nabla p = f \tag{5.8}$$

under incompressibility assumption we can rewrite it as

$$u_t + (u\cdot\nabla)u - \nu\Delta u + \nabla p = f, \quad in \quad (0,T]\times\Omega \tag{5.9}$$

which is the mostly used version of momentum equations.

Conservation of mass equations are coupled with conservation of momentum equations

$$\frac{\partial \rho}{\partial t} + \nabla \cdot (\rho u) = 0.$$

We are working with incompressible fluids means constant density, i.e. effects of pressure on the fluid density is neglected. In the equation, assuming $\frac{\partial \rho}{\partial t} = 0$, we obtain the coupled incompressibility condition

$$\nabla \cdot u = 0. \tag{5.10}$$

Together with normalization of pressure with a mean of zero, in this thesis we consider the following incompressible Navier-Stokes equations governing the blood motion;

$$\begin{aligned} u_t + (u \cdot \nabla)u - \nu \Delta u + \nabla p = f, \quad in \quad (0,T] \times \Omega \\ \nabla \cdot u = 0 \quad in \quad (0,T] \times \Omega \\ u(x,0) = u_0(x) \quad for \quad x \in \Omega \\ u = 0 \quad on \quad \Gamma_{Wall} \\ n \cdot \sigma = 0 \quad on \quad \Gamma_{out} \\ u = c \quad on \quad \Gamma_{in} \\ \int_\Omega p \, \mathrm{d}x = 0 \quad in \quad (0,T]. \end{aligned} \tag{5.11}$$

To introduce the weak form of equation (5.11), we first need to introduce the velocity and pressure spaces

$$\begin{aligned} X = H_0^1(\Omega)^d := \{v \in H^1(\Omega)^d : v|_{\partial\Omega} = 0\}, \\ Q = L_0^2(\Omega) := \{q \in L^2(\Omega) : \int_\Omega q dx = 0\}. \end{aligned}$$

The divergence free space is also defined by

$$V := \{v \in X : (q, \nabla \cdot v) = 0, \forall q \in Q\}.$$

We multiply both sides of (5.9) with $v \in X$ and integrate over the domain, then the diffusive term becomes

$$(\Delta u, v) = \int_\Omega \nabla^2 uv \, \mathrm{d}x = \int_\Omega \nabla \cdot \nabla uv \, \mathrm{d}x = \int_\Omega \nabla u \cdot \nabla v \, \mathrm{d}x + \int_{\partial\Omega} n \cdot \nabla uv \, \mathrm{d}s.$$

Similarly for the pressure term, divergence theorem and the definition of X gives

$$(\nabla p, v) = (p, \nabla \cdot v).$$

Thus multiplying (5.9) with v and incompressibility constraint (5.10) with q yields

$$(u_t, v) + \nu(\nabla u, \nabla v) + (u \cdot \nabla u, v) - (p, \nabla . v) = (f, v), \quad \forall v \in X, \tag{5.12}$$

$$(\nabla \cdot u, q) = 0, \quad \forall q \in Q.$$

To write Galerkin finite element formulation of the Navier-Stokes equations, we choose finite element spaces (X_h, Q_h) satisfying the following inf-sup (Ladyzhenskaya–Babuška–Brezzi(LBB)) condition

$$\inf_{q_h \in Q_h} \sup_{v_h \in X_h} \frac{(q_h, \nabla \cdot v_h)}{\|\nabla v_h\| \|q_h\|} \geq \beta > 0 \tag{5.13}$$

with a constant β, to ensure well-posedness of the discrete Galerkin finite element formulation [32].

Discretely divergence free space is defined as

$$V_h := \{v_h \in X_h : (q_h, \nabla \cdot v_h) = 0, \forall q_h \in Q_h\}.$$

Since $V_h \not\subset V$ in general, we cannot say that V_h is completely divergence free. Therefore we define the skew-symetric form to overcome any difficulty regarding this situation.

Lemma 5.0.1 *(Skew-symmetry) If $v \cdot n = 0$ on $\partial\Omega$, $v, \nabla v \in L^2(\Omega)$ and $\nabla \cdot v = 0$, then for such u, v, w, we have*

$$\int_\Omega u \cdot v \cdot w \, \mathrm{d}x = -\int_\Omega u \cdot w \cdot v \, \mathrm{d}x.$$

Definition 5.0.1 *The skew-symetric trilinear form is defined as*

$$b^*(u, v, w) = \frac{1}{2}((u \cdot \nabla)v, w) - \frac{1}{2}((u \cdot \nabla)w, v).$$

The following inequalities will be used through error analysis. We now state the following results.

Lemma 5.0.2 *Given that $\forall u, v, w \in X$, the following inequalities holds*

$$b^*(u, v, w) \leq M\|\nabla u\|\|\nabla v\|\|\nabla w\|,$$

$$b^*(u, v, w) \leq M\|u\|^{\frac{1}{2}}\|\nabla u\|^{\frac{1}{2}}\|\nabla v\|\|\nabla w\|.$$

Proof:

$$|b^*(u, v, w)| = \frac{1}{2}|((u \cdot \nabla)v, w)| + |\frac{1}{2}((u \cdot \nabla)w, v)| \tag{5.14}$$

By applying Hölder's inequality, we obtain

$$\leq C||u||_{L^4(\Omega)}||\nabla v||_{L^2(\Omega)}||w||_{L^4(\Omega)} + ||u||_{L^4(\Omega)}||\nabla w||_{L^2(\Omega)}||v||_{L^4(\Omega)}. \tag{5.15}$$

By using the second Ladyzenskaya inequality (4.0.1), we obtain

$$\leq \frac{4C}{3\sqrt{3}}||u||^{\frac{1}{4}}||\nabla u||^{\frac{3}{4}}||\nabla v||||w||^{\frac{1}{4}}||\nabla w||^{\frac{3}{4}} + \frac{4C}{3\sqrt{3}}||u||^{\frac{1}{4}}||\nabla u||^{\frac{3}{4}}||\nabla w||||v||^{\frac{1}{4}}||\nabla v||^{\frac{3}{4}}. \tag{5.16}$$

Finally, using Poincaré-Friedrichs inequality (4.0.2), we get

$$b^*(u, v, w) \leq M\|\nabla u\|\|\nabla v\|\|\nabla w\|.$$

Proof of the second statement follows from

$$|b^*(u, v, w)| = \frac{1}{2}|((u \cdot \nabla)v, w)| + |\frac{1}{2}((u \cdot \nabla)w, v)|. \tag{5.17}$$

By applying Hölder's inequality, we obtain

$$\leq C||u||_{L^4(\Omega)}||\nabla v||_{L^2(\Omega)}||w||_{L^4(\Omega)} + ||u||_{L^4(\Omega)}||\nabla w||_{L^2(\Omega)}||v||_{L^4(\Omega)}. \tag{5.18}$$

Next, by using the first statement in the Ladyzenskaya inequality (4.0.1), we obtain

$$\leq 2^{\frac{1}{4}}||u||^{\frac{1}{2}}||\nabla u||^{\frac{1}{2}}||\nabla v||||w||^{\frac{1}{2}}||\nabla w||^{\frac{1}{2}} + 2^{\frac{1}{4}}||u||^{\frac{1}{2}}||\nabla u||^{\frac{1}{2}}||\nabla w||||v||^{\frac{1}{2}}||\nabla v||^{\frac{1}{2}}. \tag{5.19}$$

Finally, using Poincaré-Friedrichs inequality (4.0.2), we get

$$b^*(u, v, w) \leq M\|u\|^{\frac{1}{2}}\|\nabla u\|^{\frac{1}{2}}\|\nabla v\|\|\nabla w\|.$$

□

By using the skew symmetric form, the Galerkin finite element approximation can be written as, find $(u_h, p_h) \in (X_h, Q_h)$ such that,

$$(\partial_t u_h, v_h) + \nu(\nabla u_h, \nabla v_h) + b^*(u_h, u_h, v_h) - (p_h, \nabla . v_h) = (f, v_h), \tag{5.20}$$

$$(\nabla \cdot u_h, q_h) = 0,$$

for $(v_h, q_h) \in (X_h, Q_h)$.

5.1 The Grad-div Stabilization

Although finite element discretization is a very efficient tool to numerically solve partial differential equations, this formulation may lead some instabilities in the solution of Navier-Stokes equations. In case of high Reynolds number, the flow becomes convection dominated, and it becomes turbulent. Violation of inf-sup condition is another reason for instability which causes oscillations especially in pressure field. We can overcome this by automatically choosing appropriate FE spaces satisfying this condition.

While SUPG, PSGS and VMS are most popular stabilization methods to solve first type of instability, this thesis concerns about another residual based stabilization method, grad-div stabilization, that is first introduced in [33], works by adding an extra term to weak formulization accompanied with a penalty term $\gamma(\nabla \cdot u_h, \nabla \cdot v_h)$, and helps to control the effect of pressure on velocity error due to lack of conservation. In [34], steady Stokes equations and in [35], steady Navier-Stokes equations are studied. In [36], grad-div stabilized time-dependent Oseen problem with the fully discrete and the continuous-in-time cases of backward Euler method, BDF2, and Crank–Nicolson schemes are studied for small viscosity. In [37], a grad-div stabilized fully discrete implicit Euler method is used to analyse inf-sup stable finite element discretizations of the evolutionary Navier-Stokes equations. Choice of the grad-div parameter γ is an open problem; in [38, 39], it is studied that a choice of penalty parameter of $O(1)$ is a good choice, in general. In [40], the limit of the solutions of grad-div stabilized Navier-Stokes equations with Taylor-Hood elements converges to solutions of Navier-Stokes equations with Scott-Vogelius elements, and a good performance is reported as the stabilization parameter γ goes to ∞. This implies picking large parameter γ

values would not damage the solutions.

To obtain the grad-div stabilized finite element formulation, one adds the penalty term $\gamma(\nabla \cdot u_h, \nabla \cdot v_h)$ to weak formulation (5.20), then the weak formulization of grad-div stabilized Navier-Stokes should be stated as: Find $(u_h, p_h) \in (X_h, Q_h)$ such that,

$$(\partial_t u_h, v_h) + \nu(\nabla u_h, \nabla v_h) + b^*(u_h, u_h, v_h) - (p_h, \nabla \cdot v_h) + \gamma(\nabla \cdot u_h, \nabla \cdot v_h) \\ +(\nabla \cdot u_h, q_h) = (f, v_h) \tag{5.21}$$

for $(v_h, q_h) \in (X_h, Q_h)$

In this thesis, these equations are used to approximate to the solution of Navier-Stokes equations to govern the blood flow phenomena. In our numerical experiments, we compare the effect of the grad-div stabilization parameter into finite element approximations of Navier-Stokes equations.

CHAPTER 6

NUMERICAL ANALYSIS OF THE GRAD-DIV STABILIZED NAVIER-STOKES EQUATIONS

In this chapter, we present a finite element approximation of time dependent Navier-Stokes equations using backward Euler's method. First, we present the stability analysis of the grad-div stabilized Navier-Stokes equations with fully discrete scheme using backward Euler's method, then discuss existence and uniqueness of the approximate solution. Then we present error analysis of the same scheme. Let us first present the fully discretized Navier-Stokes equations with grad-div stabilization.

Let the time interval $[0, T]$ is discretized by $0 = t_0 < t_1 < ... < t_N = T < \infty$ with $\Delta t = t_n - t_{n-1}$, $(u_n^h, p_n^h) \in (X_h, Q_h)$ are approximations of the pressure and the velocity. Given u_n^h, we have the time discrete problem: find (u_{n+1}^h, p_{n+1}^h) such that

$$\begin{aligned}(\frac{u_{n+1}^h - u_n^h}{\Delta t}, v^h) + \nu(\nabla u_{n+1}^h, \nabla v_h) + b^*(u_{n+1}^h, u_{n+1}^h, v_h) + (p_{n+1}^h, \nabla \cdot u_n^h) \\ -(\nabla \cdot u_{n+1}^h, q^h) + \gamma(\nabla \cdot u_{n+1}^h, \nabla \cdot v^h) = (f_{n+1}, v^h)\end{aligned} \tag{6.1}$$

for all $(v^h, q^h) \in (X_h, Q_h)$.

For numerical analysis, we consider the equivalent formulation in V^h. We note that, under inf-sup condition (5.13), the following formulation

$$\begin{aligned}&(\frac{u_{n+1}^h - u_n^h}{\Delta t}, v^h) + \nu(\nabla u_{n+1}^h, \nabla v_h) + b^*(u_{n+1}^h, u_{n+1}^h, v_h) + \gamma(\nabla \cdot u_{n+1}^h, \nabla \cdot v^h) \\ &= (f_{n+1}, v^h)\end{aligned} \tag{6.2}$$

for all $v^h \in V^h$, and the formulation (6.1) in X^h are equivalent. We note that, numerical analysis of the grad-div stabilized Navier-Stokes equations has been studied

extensively in [36, 37, 40]. We now review this analysis.

6.1 Stability Analysis

Lemma 6.1.1 *(Stability of the Solutions) Let $f \in L^2(0,T;H^{-1}(\Omega))$,the scheme (6.2) is unconditionally stable, and for any $h, k, \gamma > 0$, it satisfies the following bound:*

$$\frac{1}{2}\|u_N^h\|^2+\frac{\nu\Delta t}{2}\sum_{n=0}^{N-1}\|\nabla u_{n+1}^h\|^2+\gamma\Delta t\sum_{n=0}^{N-1}\|\nabla\cdot u_{n+1}^h\|^2 \leq \frac{1}{2}\|u_0^h\|^2+\frac{\Delta t}{2\nu}\sum_{n=0}^{N-1}\|f_{n+1}\|_{-1}^2$$

Proof: Suppose that u_n^h and p_n^h are approximations of velocity and pressure respectively. In (6.2) let $v_h = u_{n+1}^h$ and $q^h = p_{n+1}^h$, we get

$$(u_{n+1}^h, u_{n+1}^h) - (u_n^h, u_{n+1}^h) + \Delta t\nu(\nabla u_{n+1}^h, \nabla u_{n+1}^h) + \gamma\Delta t(\nabla\cdot u_{n+1}^h, \nabla\cdot u_{n+1}^h) = \Delta t(f_{n+1}, u_{n+1}^h).$$

Application of Cauchy-Schwarz inequality (4.0.3) and definition of norms gives

$$\|u_{n+1}^h\|^2+\Delta t\nu\|\nabla u_{n+1}^h\|^2+\gamma\Delta t\|\nabla\cdot u_{n+1}^h\|^2 \leq |\Delta t(f_{n+1}, u_{n+1}^h)|+|(u_n^h, u_{n+1}^h)|. \quad (6.3)$$

To bound right hand side, we use the definition of the dual norm (4.0.7) on Young's inequality (4.0.8)

$$(f_{n+1}, u_{n+1}^h) \leq \|f\|_{-1}\|\nabla u_{n+1}^h\| \leq \frac{1}{2\nu}\|f\|_{-1}^2 + \frac{\nu}{2}\|\nabla u_{n+1}^h\|^2.$$

Applying Cauchy Schwards inequality and Young's inequality gives

$$(u_n^h, u_{n+1}^h) \leq \frac{1}{2}\|u_n^h\| + \frac{1}{2}\|u_{n+1}^h\|.$$

Substitute this last estimate in (6.3) we get the following inequality

$$\frac{1}{2}\|u_{n+1}^h\|^2 - \frac{1}{2}\|u_n^h\|^2 + \frac{\nu\Delta t}{2}\|\nabla u_{n+1}^h\|^2 + \gamma\Delta t\|\nabla\cdot u_{n+1}^h\|^2 \leq \frac{\Delta t}{2\nu}\|f_{n+1}\|_{-1}^2.$$

Summing over times steps from $n = 0$ to $N-1$, we obtain

$$\frac{1}{2}\|u_N^h\|^2+\frac{\nu\Delta t}{2}\sum_{n=0}^{N-1}\|\nabla u_{n+1}^h\|^2+\gamma\Delta t\sum_{n=0}^{N-1}\|\nabla\cdot u_{n+1}^h\|^2 \leq \frac{1}{2}\|u_0^h\|^2+\frac{\Delta t}{2\nu}\sum_{n=0}^{N-1}\|f_{n+1}\|_{-1}^2.$$

Corollary 6.1.1 *Lemma 6.1.1 implies that the approximate solution u_n^h is bounded by data. Thus, the velocity solution exists and unique. For pressure, the inf-sup condition implies that, the pressure solution exists and unique [41].*

6.2 Error Analysis

Along with the discrete inf-sup condition, we also assume the following approximations hold for our choice of the velocity-pressure spaces [42]

$$\begin{aligned}
\inf_{v_h \in X^h} \|u - v_h\| &\leq Ch^{k+1}|u|_{k+1}, u \in H^{k+1}(\Omega)^d, \\
\inf_{q_h \in Q^h} \|p - q_h\| &\leq Ch^{s+1}|u|_{s+1}, p \in H^{s+1}(\Omega)^d, \\
\inf_{v \in X^h} \|\nabla(u - v_h)\| &\leq Ch^{k}|u|_{k+1}, u \in H^{k+1}(\Omega)^d.
\end{aligned} \tag{6.4}$$

We also adopt the following discrete norms:

$$|||v|||_{\infty,k} := \max_{0 \leq n \leq N_T} \|v_n\|_k,$$

$$|||v|||_{p,k} := (\Delta t \sum_{n=0}^{N_T} \|v_n\|_k^p)^{\frac{1}{p}},$$

and regularity assumptions

$$u \in L^4(0,T; H^{k+1}(\Omega)^d) \cap L^4(0,T; L^2(\Omega)) \cap L^\infty(0,T; L^2(\Omega)),$$

$$p \in L^2(0,T; H^{s+1}(\Omega)),$$

$$u_t \in L^\infty(0,T; L^2(\Omega)).$$

Lemma 6.2.1 *(Error analysis) Let (u,p) be solution of Navier-Stokes equations (5.11), then the error $e = u(t_n) - u_n^h$ of the scheme (6.2) satisfies the following bound:*

$$\begin{aligned}
&\|e_N\|^2 + \sum_{n=0}^{N-1} \|e_{n+1} - e_n\| + \frac{\nu}{2}\Delta t \sum_{n=0}^{N-1} \|\nabla e_{n+1}\|^2 + \frac{\Delta t \gamma}{2} \sum_{n=0}^{N-1} \|\nabla \cdot e_{n+1}\|^2 \\
&\leq \|e_0\|^2 + C(\nu+\gamma)h^{2k}|||u|||_{2,k+1}^2 + Ch^{2k+1}\nu^{-1}(|||u|||_{4,k+1}^4 + |||\nabla u|||_{4,0}^4) \\
&\quad + Ch^{2k}\nu^{-1}(|||u|||_{4,k+1}^4 + \nu^{-1}(\|u^h\|^2 + \nu^{-1}|||f|||_{2,-1}^2)) \\
&\quad + \Delta t \sum_{n=0}^{N-1} C\nu^{-1}\|p_{n+1} - q^h\|^2 + Ch^{2k+2}(|||u|||_{2,k+1}^2) \\
&\quad + \sum_{n=0}^{N-1} \frac{(\Delta t)^2}{6}(\int_{t_n}^{t_{n+1}} \|\partial_{tt} u\|^2 \, \mathrm{d}t).
\end{aligned}$$

Proof:

Let us denote the true solution of Navier-Stokes equations $u_{n+1} = u(t_{n+1})$ at $t = t_{n+1}$. Subtracting the true solution of Navier-Stokes equations at $t = t_{n+1}$ from (6.2), we obtain

$$\begin{aligned}&(\partial_t u_{n+1} - \frac{u^h_{n+1} - u^h_n}{\Delta t}, v^h) + b^*(u_{n+1}, u_{n+1}, v^h) - b^*(u^h_{n+1}, u^h_{n+1}, v^h)\\ &+ \nu(\nabla(u_{n+1} - u^h_{n+1}), \nabla v^h) + (p_{n+1} - q^h, \nabla \cdot v^h) + \gamma(\nabla \cdot (u_{n+1} - u^h_{n+1}), \nabla \cdot v^h)\\ &= (f_{n+1}, v^h).\end{aligned} \tag{6.5}$$

Further, adding and subtracting terms gives

$$\begin{aligned}(\partial_t u_{n+1} - \frac{u^h_{n+1} - u^h_n}{\Delta t}, v^h) &= (\partial_t u_{n+1} + \frac{u_{n+1} - u_n}{\Delta t} - \frac{u_{n+1} - u_n}{\Delta t} - \frac{u^h_{n+1} - u^h_n}{\Delta t}, v^h)\\ &= (\frac{e_{n+1} - e_n}{\Delta t}, v^h) + (\partial_t u_{n+1} - \frac{u_{n+1} - u_n}{\Delta t}, v^h)\end{aligned}$$

Then, the equation (6.5) can be written as

$$\begin{aligned}&(\frac{e_{n+1} - e_n}{\Delta t}, v^h) + b^*(u_{n+1}, u_{n+1}, v^h) - b^*(u^h_{n+1}, u^h_{n+1}, v^h) + \nu(\nabla e_{n+1}, \nabla v^h)\\ &+ (\nabla \cdot v^h, p_{n+1} - q^h) + \gamma(\nabla \cdot e_{n+1}, \nabla \cdot v^h) = (f_{n+1}, v^h) + \tau(u_n, v^h)\end{aligned} \tag{6.6}$$

with the consistency error term

$$\tau(u_n, v^h) = (\partial_t u_{n+1} - \frac{u_{n+1} - u_n}{\Delta t}, v^h).$$

Decomposing error as

$$e_n = (u_n - U_n) - (u^h_n - U_n) = \eta_n - \phi^h_n$$

where U_n is approximation of u_n in V^h. Then, set $v^h = \phi^h_{n+1}$ in (6.6), we obtain

$$\begin{aligned}&(\frac{\eta_{n+1} - \eta_n}{\Delta t}, \phi^h_{n+1}) + (\frac{\phi^h_{n+1} - \phi^h_n}{\Delta t}, \phi^h_{n+1}) + b^*(u_{n+1}, u_{n+1}, \phi^h_{n+1})\\ &- b^*(u^h_{n+1}, u^h_{n+1}, \phi^h_{n+1}) + \nu(\nabla(\eta_{n+1} - \phi^h_{n+1}), \nabla\phi^h_{n+1}) = (p_{n+1} - q^h, \nabla \cdot \phi^h_{n+1})\\ &- \gamma(\nabla \cdot (\eta_{n+1} - \phi^h_{n+1}), \nabla \cdot \phi^h_{n+1}) + \tau(u_n, \phi^h_{n+1}).\end{aligned} \tag{6.7}$$

Using $a^2 - ab = \frac{a^2+(a-b)^2-b^2}{2}$, it follows that

$$(\phi_{n+1}^h - \phi_n^h, \phi_{n+1}^h) = \frac{1}{2}(\|\phi_{n+1}^h\|^2 + \|\phi_{n+1}^h - \phi_n^h\|^2 - \|\phi_n^h\|^2).$$

Also using Cauchy-Schwarz inequality and definition of norms gives

$$\begin{aligned}
&\frac{1}{2\Delta t}(\|\phi_{n+1}^h\|^2 + \|\phi_{n+1}^h - \phi_n^h\|^2 - \|\phi_n^h\|^2) + \nu\|\nabla\phi_{n+1}^h\|^2 + \frac{\gamma}{2}\|\nabla\cdot\phi_{n+1}^h\|^2 \\
&= \nu(\nabla\eta_{n+1}, \nabla\phi_{n+1}^h) + b^*(u_{n+1}, u_{n+1}, \phi_{n+1}^h) - b^*(u_{n+1}^h, u_{n+1}^h, \phi_{n+1}^h) \\
&+ (\nabla\cdot v^h, p_{n+1} - q^h) - \gamma(\nabla\cdot\eta_{n+1}, \nabla\cdot\phi_{n+1}^h) - (\eta_{n+1} - \eta_n, \phi_{n+1}^h) + \tau(u_n, \phi_{n+1}^h).
\end{aligned} \tag{6.8}$$

For the nonlinear terms, we add and subtract terms as:

$$\begin{aligned}
&b^*(u_{n+1}, u_{n+1}, v^h) - b^*(u_{n+1}^h, u_{n+1}^h, v^h) \\
&= b^*(u_{n+1}, u_{n+1}, v^h) + b^*(u_{n+1}^h, u_{n+1}, v^h) - b^*(u_{n+1}^h, u_{n+1}, v^h) - b^*(u_{n+1}^h, u_{n+1}^h, v^h) \\
&= b^*(u_{n+1}^h, \eta_{n+1} - \phi_{n+1}^h, \phi_{n+1}^h) + b^*(\eta_{n+1} - \phi_{n+1}^h, u_{n+1}, \phi_{n+1}^h) \\
&= b^*(u_{n+1}^h, \eta_{n+1}, \phi_{n+1}^h) - b^*(u_{n+1}^h, \phi_{n+1}^h, \phi_{n+1}^h) \\
&+ b^*(\eta_{n+1}, u_{n+1}, \phi_{n+1}^h) - b^*(\phi_{n+1}^h, u_{n+1}, \phi_{n+1}^h).
\end{aligned} \tag{6.9}$$

Using skew symmetry property $b^*(u_{n+1}^h, \phi_{n+1}^h, \phi_{n+1}^h) = 0$, and substituting this in (6.9) gives

$$\begin{aligned}
&\frac{1}{2\Delta t}(\|\phi_{n+1}^h\|^2 + \|\phi_{n+1}^h - \phi_n^h\|^2 - \|\phi_n^h\|^2) + \nu\|\nabla\phi_{n+1}^h\|^2 + \frac{\gamma}{2}\|\nabla\cdot\phi_{n+1}^h\|^2 \\
&= \nu(\nabla\eta_{n+1}, \nabla\phi_{n+1}^h) + (\nabla\cdot v^h, p_{n+1} - q^h) - \gamma(\nabla\cdot\eta_{n+1}, \nabla\cdot\phi_{n+1}^h) \\
&- b^*(\eta_{n+1}, u_{n+1}, \phi_{n+1}^h) + b^*(\phi_{n+1}^h, u_{n+1}, \phi_{n+1}^h) - b^*(u_{n+1}^h, \eta_{n+1}, \phi_{n+1}^h) \\
&- (\eta_{n+1} - \eta_n, \phi_{n+1}^h) + \tau(u_n, \phi_{n+1}^h).
\end{aligned} \tag{6.10}$$

We now bound all of the terms in the right hand side of (6.10). For $\nu(\nabla\eta_{n+1}, \nabla\phi_{n+1}^h)$, using Cauchy-Schwarz and Young's inequalities gives

$$\nu(\nabla\eta_{n+1}, \nabla\phi_{n+1}^h) \le \nu\|\nabla\eta_{n+1}\|\|\nabla\phi_{n+1}^h\| \le \frac{\nu}{12}\|\nabla\phi_{n+1}^h\|^2 + C\nu\|\nabla\eta_{n+1}\|^2.$$

For the term $(p_{n+1} - q^h, \nabla\cdot\phi_{n+1}^h)$, using Cauchy-Schwarz inequality and Lemma (4.0.3)

$$(p_{n+1} - q^h, \nabla\cdot\phi_{n+1}^h) \le C\|p_{n+1} - q^h\|\|\nabla\phi_{n+1}^h\| \le \frac{\nu}{12}\|\nabla\phi_{n+1}^h\|^2 + C\nu^{-1}\|p_{n+1} - q^h\|^2.$$

Similarly for the term $\gamma(\nabla\cdot\eta_{n+1}, \nabla\cdot\phi_{n+1}^h)$, using Cauchy-Schwarz inequality and Lemma (4.0.3)

$$\gamma(\nabla\cdot\eta_{n+1}, \nabla\cdot\phi_{n+1}^h) \le \frac{\gamma}{2}\|\nabla\cdot\phi_{n+1}^h\|^2 + \gamma C\|\nabla\eta_{n+1}\|^2$$

To bound nonlinear terms, we first use Lemma (5.0.2) and Young's inequalities

$$\begin{aligned} &b^*(\eta_{n+1}, u_{n+1}, \phi^h_{n+1}) \leq C\|\eta_{n+1}\|^{\frac{1}{2}}\|\nabla\eta_{n+1}\|^{\frac{1}{2}}\|\nabla u_{n+1}\|\|\nabla\phi^h_{n+1}\| \\ &\leq \frac{\nu}{12}\|\nabla\phi^h_{n+1}\|^2 + C\nu^{-1}\|\eta_{n+1}\|\|\nabla\eta_{n+1}\|\|\nabla u_{n+1}\|^2. \end{aligned} \tag{6.11}$$

Similarly we get

$$\begin{aligned} &b^*(\phi^h_{n+1}, u_{n+1}, \phi^h_{n+1}) \leq C\|\phi^h_{n+1}\|^{\frac{1}{2}}\|\nabla\phi^h_{n+1}\|^{\frac{1}{2}}\|\nabla u_{n+1}\|\|\nabla\phi^h_{n+1}\| \\ &\leq C\|\phi^h_{n+1}\|^{\frac{1}{2}}\|\nabla\phi^h_{n+1}\|^{\frac{3}{2}}\|\nabla u_{n+1}\|. \end{aligned} \tag{6.12}$$

Using (4.0.8), picking $p = 4$ and $q = \frac{4}{3}$, we get

$$\leq \frac{\nu}{12}\|\nabla\phi^h_{n+1}\|^2 + C\nu^{-3}\|\phi^h_{n+1}\|^2\|\nabla u_{n+1}\|^4.$$

For the last nonlinear term, again using (5.0.2) and Young's inequality yields

$$\begin{aligned} &b^*(u^h_{n+1}, \eta_{n+1}, \phi^h_{n+1}) \leq C\|u^h_{n+1}\|^{\frac{1}{2}}\|\nabla u^h_{n+1}\|^{\frac{1}{2}}\|\nabla\eta_{n+1}\|\|\nabla\phi^h_{n+1}\| \\ &\leq \frac{\nu}{12}\|\nabla\phi^h_{n+1}\|^2 + C\nu^{-1}\|u^h_{n+1}\|\|\nabla u^h_{n+1}\|\|\nabla\eta_{n+1}\|^2. \end{aligned} \tag{6.13}$$

Finally for the term $(\eta_{n+1}-\eta_n, \phi^h_{n+1})$, using Cauchy-Schwarz, Young's and Poincaré-Friedrichs inequalities gives,

$$(\eta_{n+1} - \eta_n, \phi^h_{n+1}) \leq \|\eta_{n+1} - \eta_n\|\|\phi^h_{n+1}\|,$$

$$\leq C\nu^{-1}\|\eta_{n+1} - \eta_n\|^2 + \frac{\nu}{12}\|\nabla\phi^h_{n+1}\|^2,$$

$$\leq C\nu^{-1}(\|\eta_{n+1}\|^2 + \|\eta_n\|^2) + \frac{\nu}{12}\|\nabla\phi^h_{n+1}\|^2.$$

Combining all the estimates, we obtain the following inequality

$$\begin{aligned} &\frac{1}{2\Delta t}(\|\phi^h_{n+1}\|^2 + \|\phi^h_{n+1} - \phi^h_n\|^2 - \|\phi^h_n\|^2) + \frac{\nu}{2}\|\nabla\phi^h_{n+1}\|^2 + \frac{\gamma}{2}\|\nabla\cdot\phi^h_{n+1}\|^2 \\ &\leq C(\nu+\gamma)\|\nabla\eta_{n+1}\|^2 + C\nu^{-1}\|p_{n+1} - q^h\|^2 + C\nu^{-1}\|\eta_{n+1}\|\|\nabla\eta_{n+1}\|\|\nabla u_{n+1}\|^2 \\ &+ C\nu^{-3}\|\phi^h_{n+1}\|^2\|\nabla u_{n+1}\|^4 + C\nu^{-1}\|u^h_{n+1}\|\|\nabla u^h_{n+1}\|\|\nabla\eta_{n+1}\|^2 \\ &+ \|\eta_{n+1}\|^2 + \|\eta_n\|^2 + \tau(u_h, \phi^h_{n+1}), \end{aligned} \tag{6.14}$$

and summing from $n = 0$ to $N - 1$, we obtain

$$\begin{aligned}
&\frac{1}{2}\|\phi^h_{N-1}\|^2 + \frac{1}{2}\sum_{n=0}^{N-1}\|\phi^h_{n+1} - \phi^h_n\|^2 + \frac{\nu}{2}\Delta t\sum_{n=0}^{N-1}\|\nabla\phi^h_{n+1}\|^2 + \frac{\Delta t\gamma}{2}\sum_{n=0}^{N-1}\|\nabla\cdot\phi^h_{n+1}\|^2 \\
&\leq \frac{1}{2}\|\phi_0\|^2 + \Delta t\sum_{n=0}^{N-1}C\nu^{-3}\|\nabla u_{n+1}\|^4\|\phi^h_{n+1}\|^2 + \Delta t\sum_{n=0}^{N-1}(C\nu + C\gamma)\|\nabla\eta_{n+1}\|^2 \\
&+ \Delta t\sum_{n=0}^{N-1}C\nu^{-1}\|\eta_{n+1}\|\|\nabla\eta_{n+1}\|\|\nabla u_{n+1}\|^2 + \Delta t\sum_{n=0}^{N-1}C\nu^{-1}\|u^h_{n+1}\|\|\nabla u^h_{n+1}\|\|\nabla\eta_{n+1}\|^2 \\
&+ \Delta t\sum_{n=0}^{N-1}C\nu^{-1}\|p_{n+1} - q^h\|^2 + \Delta t\sum_{n=0}^{N-1}(\|\eta_{n+1}\|^2 + \|\eta_n\|^2) + \Delta t\sum_{n=0}^{N-1}|\tau(u_h, \phi^h_{n+1})|.
\end{aligned} \tag{6.15}$$

We continue the proof by estimating right hand side of the inequality. Using assumption (6.4),

$$\begin{aligned}
&\Delta t\sum_{n=0}^{N-1}(C(\nu+\gamma))\|\nabla\eta_{n+1}\|^2 \leq \Delta t(C(\nu+\gamma))\sum_{n=0}^{N}\|\nabla\eta_n\|^2 \\
&\leq \Delta t C(\nu+\gamma)\sum_{n=0}^{N}h^{2k}|u_n|^2_{k+1} \\
&\leq C(\nu+\gamma)h^{2k}|||u|||^2_{2,k+1}.
\end{aligned} \tag{6.16}$$

We also have the term

$$\Delta t\sum_{n=0}^{N-1}C\nu^{-1}\|\eta_{n+1}\|\|\nabla\eta_{n+1}\|\|\nabla u_{n+1}\|^2$$

$$\leq Ch^{2k+1}\nu^{-1}\left\{\Delta t\sum_{n=0}^{N-1}|u_{n+1}|^2\|\nabla u_{n+1}\|^2\right\}$$

Then using the the Cauchy-Schwarz and Young's inequalities,

$$\leq Ch^{2k+1}\nu^{-1}(\Delta t\sum_{n=0}^{N}|u_n|^4)^{\frac{1}{2}}(\Delta t\sum_{n=0}^{N}\|\nabla u_n\|^4)^{\frac{1}{2}}$$

$$\leq Ch^{2k+1}\nu^{-1}(|||u|||^4_{4,k+1} + |||\nabla u|||^4_{4,0}).$$

For the other term, using the estimate for $\|u^h_n\|$ in stability Lemma 6.1.1,

$$\Delta t\sum_{n=0}^{N-1}C\nu^{-1}\|u^h_{n+1}\|\|\nabla u^h_{n+1}\|\|\nabla\eta_{n+1}\|^2 \leq \Delta t C\nu^{-1}\sum_{n=0}^{N-1}\|\nabla u^h_{n+1}\|\|\nabla\eta_{n+1}\|^2$$

and using assumption (6.4), we get

$$\leq Ch^{2k}\nu^{-1}\left\{\Delta t\sum_{n=0}^{N-1}|u_{n+1}|_{k+1}^{2}\|\nabla u_{n+1}^{h}\|\right\}.$$

Using Cauchy-Schwarz and Young's inequalities, we obtain the following bounds

$$\leq Ch^{2k}\nu^{-1}(\Delta t\sum_{n=0}^{N-1}|u_{n+1}|_{k+1}^{4})^{\frac{1}{2}}(\Delta t\sum_{n=0}^{N-1}\|\nabla u_{n+1}^{h}\|^{2})^{\frac{1}{2}}$$

$$\leq Ch^{2k}\nu^{-1}(|||u|||_{4,k+1}^{4}+\Delta t\sum_{n=0}^{N}\|\nabla u_{n}^{h}\|^{2})$$

$$\leq Ch^{2k}\nu^{-1}(|||u|||_{4,k+1}^{4}+\nu^{-1}(\|u^{h}\|^{2}+\nu^{-1}|||f|||_{2,-1}^{2}).$$

and using Young's inequality, we get the following bound,

$$\leq Ch^{k+1}(|||u|||_{2,k+1}^{2}+\Delta t\sum_{n=0}^{N-1}\|\phi_{n+1}^{h}\|^{2}) \quad .$$

In addition, for the next term we use the assumption (6.4) and obtain

$$\Delta t\sum_{n=0}^{N-1}(\|\eta_{n+1}\|+\|\eta_{n}\|)\|\phi_{n+1}^{h}\|\leq h^{k+1}\Delta t\sum_{n=0}^{N-1}(|u_{n+1}|_{k+1}+|u_{n}|)_{k+1}\|\phi_{n+1}^{h}\|$$

$$\Delta t\sum_{n=0}^{N-1}(\|\eta_{n+1}\|^{2}+\|\eta_{n}\|^{2})\leq Ch^{2k+2}(|||u|||_{2,k+1}^{2}).$$

Finally, to further investigate the consistency error, using fundamental theorem of calculus and integration by parts, one has

$$u_{n}=u_{n+1}-\Delta t\partial_{t}u_{n+1}+\int_{t_{n}}^{t_{n+1}}(t-t_{n})\partial_{tt}u\,\mathrm{d}t,$$

$$\partial_{t}u_{n+1}-\frac{u_{n+1}-u_{n}}{\Delta t}=\frac{1}{\Delta t}\int_{t_{n}}^{t_{n+1}}(t-t_{n})\partial_{tt}u\,\mathrm{d}t.$$

For the consistency error, we first use Cauchy-Schwarz and Young's inequality along

with Taylor remainder term.

$$\tau(u_n,\phi^h_{n+1}) = (\partial_t u_{n+1} - \frac{u_{n+1}-u_n}{\Delta t}, \phi^h_{n+1}) \le \|\partial_t u_{n+1} - \frac{u_{n+1}-u_n}{\Delta t}\|\|\phi^h_{n+1}\|$$
$$\le \frac{1}{2}\|\frac{u_{n+1}-u_n}{\Delta t} - u_t(t_{n+1})\|^2 + \frac{1}{2}\|\phi^h_{n+1}\|^2$$
$$\le \frac{1}{2}\|\frac{1}{\Delta t}\int_{t_n}^{t_{n+1}}(t-t_n)(\partial_{tt}u)\,\mathrm{d}t\|^2 + \frac{1}{2}\|\phi^h_{n+1}\|^2$$
$$\le \frac{1}{2\Delta t^2}\|(\int_{t_n}^{t_{n+1}}(t-t_n)^2\,\mathrm{d}t)^{\frac{1}{2}}(\int_{t_n}^{t_{n+1}}\partial_{tt}u\,\mathrm{d}t)^{\frac{1}{2}}\|^2 + \frac{1}{2}\|\phi^h_{n+1}\|^2$$
$$\le \frac{1}{2\Delta t^2}(\int_{t_n}^{t_{n+1}}(t-t_n)^2\,\mathrm{d}t)(\int_\Omega\int_{t_n}^{t_{n+1}}\partial_{tt}u\,\mathrm{d}t\mathrm{d}x) + \frac{1}{2}\|\phi^h_{n+1}\|^2$$
$$\le \frac{\Delta t}{6}(\int_{t_n}^{t_{n+1}}\int_\Omega \partial_{tt}u\mathrm{d}x\,\mathrm{d}t) + \frac{1}{2}\|\phi^h_{n+1}\|^2 \le \frac{1}{2}\|\phi^h_{n+1}\|^2 + \frac{\Delta t}{6}\left(\int_{t_n}^{t_{n+1}}\|\partial_{tt}u\|^2\,\mathrm{d}t\right). \tag{6.17}$$

Substituting all the estimates, we obtain

$$\frac{1}{2}\|\phi^h_M\|^2 + \frac{1}{2}\sum_{n=0}^{N-1}\|\phi^h_{n+1}-\phi^h_n\| + \frac{\nu}{2}\Delta t\sum_{n=0}^{N-1}\|\nabla\phi^h_{n+1}\|^2 + \frac{\Delta t\gamma}{2}\sum_{n=0}^{N-1}\|\nabla\cdot\phi^h_{n+1}\|^2$$
$$\le \frac{1}{2}\|\phi_0\|^2 + \Delta t\sum_{n=0}^{N-1}C\nu^{-3}\|\nabla u_{n+1}\|^4\|\phi^h_{n+1}\|^2 + C(\nu+\gamma)h^{2k}|||u|||^2_{2,k+1}$$
$$+ Ch^{2k+1}\nu^{-1}(|||u|||^4_{4,k+1} + |||\nabla u|||^4_{4,0})$$
$$+ Ch^{2k}\nu^{-1}(|||u|||^4_{4,k+1} + \nu^{-1}(\|u^h\|^2 + \nu^{-1}|||f|||^2_{2,-1})) + \Delta t\sum_{n=0}^{N-1}C\nu^{-1}\|p_{n+1}-q^h\|^2$$
$$+ Ch^{2k+2}|||u|||^2_{2,k+1} + \Delta t\sum_{n=0}^{N-1}\frac{1}{2}\|\phi^h_{n+1}\|^2 + \sum_{n=0}^{N-1}\frac{(\Delta t)^2}{6}\left(\int_{t_n}^{t_{n+1}}\|\partial_{tt}u\|^2\,\mathrm{d}t\right). \tag{6.18}$$

Combining the right hand side,

$$\frac{1}{2}\|\phi^h_M\|^2 + \frac{1}{2}\sum_{n=0}^{N-1}\|\phi^h_{n+1}-\phi^h_n\| + \frac{\nu}{2}\Delta t\sum_{n=0}^{N-1}\|\nabla\phi^h_{n+1}\|^2 + \frac{\Delta t\gamma}{2}\sum_{n=0}^{N-1}\|\nabla\cdot\phi^h_{n+1}\|^2$$
$$\le \frac{1}{2}\|\phi_0\|^2 + \Delta t\sum_{n=0}^{N-1}(C\nu^{-3}\|\nabla u_{n+1}\|^4 + \frac{1}{2})\|\phi^h_{n+1}\|^2 + C(\nu+\gamma)h^{2k}|||u|||^2_{2,k+1}$$
$$+ Ch^{2k+1}\nu^{-1}(|||u|||^4_{4,k+1} + |||\nabla u|||^4_{4,0})$$
$$+ Ch^{2k}\nu^{-1}(|||u|||^4_{4,k+1} + \nu^{-1}(\|u^h\|^2 + \nu^{-1}|||f|||^2_{2,-1})) + \Delta t\sum_{n=0}^{N-1}C\nu^{-1}\|p_{n+1}-q^h\|^2$$
$$+ Ch^{2k+2}(|||u|||^2_{2,k+1}) + \sum_{n=0}^{N-1}\frac{(\Delta t)^2}{6}\left(\int_{t_n}^{t_{n+1}}\|\partial_{tt}u\|^2\,\mathrm{d}t\right). \tag{6.19}$$

Now let

$$G_k = exp(\sum_{n=0}^{K} \frac{K_n}{1 - \Delta t K_n})$$

and

$$K_n = (\nu^{-3}\|\nabla u_{n+1}\|^4 + \frac{1}{2})$$

Assuming $\Delta t K_n < 1$, applying discrete Gronwall lemma (4.0.4), we obtain

$$\begin{aligned}
&\frac{1}{2}\|\phi_M^h\|^2 + \frac{1}{2}\sum_{n=0}^{N-1}\|\phi_{n+1}^h - \phi_n^h\| + \frac{\nu}{2}\Delta t\sum_{n=0}^{N-1}\|\nabla\phi_{n+1}^h\|^2 + \frac{\Delta t\gamma}{2}\sum_{n=0}^{N-1}\|\nabla\cdot\phi_{n+1}^h\|^2 \\
&\leq \frac{1}{2}\|\phi_0\|^2 + C(\nu+\gamma)h^{2k}|||u|||_{2,k+1}^2 + Ch^{2k+1}\nu^{-1}(|||u|||_{4,k+1}^4 + |||\nabla u|||_{4,0}^4) \\
&+ Ch^{2k}\nu^{-1}(|||u|||_{4,k+1}^4 + \nu^{-1}(\|u^h\|^2 + \nu^{-1}|||f|||_{2,-1}^2)) + \Delta t\sum_{n=0}^{N-1} C\nu^{-1}\|p_{n+1} - q^h\|^2 \\
&+ Ch^{2k+2}(|||u|||_{2,k+1}^2) + \sum_{n=0}^{N-1}\frac{(\Delta t)^2}{6}\left(\int_{t_n}^{t_{n+1}}\|\partial_{tt}u\|^2\,\mathrm{d}t\right).
\end{aligned} \tag{6.20}$$

Using triangle inequality,

$$\|e_n\| = \|\eta_n - \phi_n^h\| \leq \|\eta_n\| + \|\phi_n^h\|$$

yields the stated result.

Remark 6.2.1 *The error analysis states that, as $h, \Delta t \to 0$ approximate solutions u_n^h converges to true solution.*

CHAPTER 7

NUMERICAL EXPERIMENTS

In this chapter, we introduce the application of Navier-Stokes equations with grad-div stabilization to investigate its effect on flow patterns on different types of pathologies of cardiovascular system, such as different shapes of stenosis and aneurysm.

We first apply the steady Navier-Stokes equations to investigate the effect of grad-div term in Section 7.1, and verify behavior of blood flow phenomena. We then apply grad-div stabilized time dependent Navier-Stokes equations in Section 7.2. Finally, we introduce periodic boundary conditions on the time dependent Navier-Stokes equations to investigate the pulsatile nature of the blood in Section 7.3.

In this thesis, all the simulations are made using Freefem++ [43]. In the experiments;

- Blood density(ρ) assumed to be constant with $1060\frac{kg}{m^3}$
- Blood viscosity(μ) assumed to be constant with $0.0035mPa \cdot s$.
- Therefore blood assumed to be a Newtonian fluid.
- Blood temperature assumed to be constant, body temperature.
- Blood assumed to be an incompressible fluid.
- No-slip boundary condition is imposed at artery walls.
- The inlet velocity is taken

  $$c = \frac{Re\mu}{\rho l}$$

  where l is the lumen diameter and Re is Reynolds number and is taken as a control parameter.

- Inf-sup stable Taylor-Hood $(P2, P1)$ elements are used for all the discretizations. Grad-div stabilized backward Euler time scheme is applied for finite element discretization of time dependent Navier-Stokes equations.

7.1 Steady Navier-Stokes Equations With Grad-div Stabilization

For problems in subsections 7.1.1 to 7.1.5, the steady Navier-Stokes equations are given as;

$$\begin{aligned} -\nu\Delta u + (u \cdot \nabla)u + \nabla p = f, \quad in \quad \Omega \\ \nabla \cdot u = 0 \quad in \quad \Omega \end{aligned} \tag{7.1}$$

In [44], stenosis, shifted stenosis and narrow stenosis are studied with velocity magnitudes and pressure profiles. For the problems from Section 7.1.1 to 7.1.5, we have used the similar geometry with different parameters, therefore we investigate more complex domains and more advanced problems, together with wall shear stress values.

For the problems in Sections 7.1.1, 7.1.2 and 7.1.3 we introduced stenosis geometries. In this geometries, the expectation is to observe increased velocity magnitudes and decreased pressure, together with increased wall shear stress values around the stenosis. For the problems in Sections 7.1.4 and 7.1.5, we introduce aneurysm geometries. The expectation is to observe smaller velocity magnitudes and wall shear stress values, together with increased pressure values around the aneurysm dilation.

7.1.1 Eccentric Stenosis

In [44], concentric stenosis problem is investigated. We have changed the geometry with a one sided geometry to investigate its effect on both the straight wall and the constrained wall.

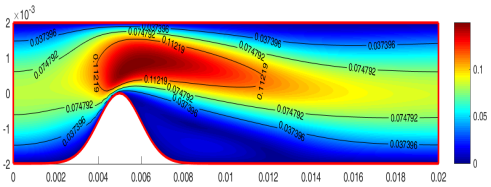

(a) $Re = 100$

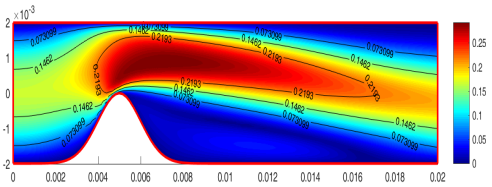

(b) $Re = 200$

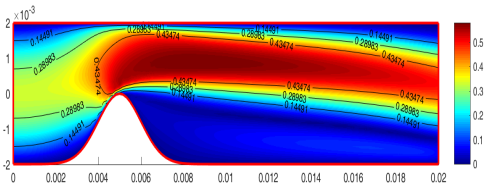

(c) $Re = 400$

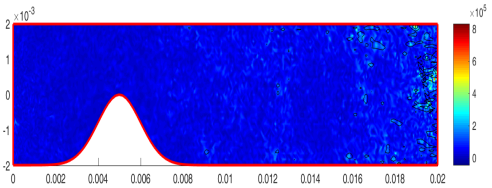

(d) $Re = 600$

Figure 7.1: Velocity magnitudes for $\gamma = 1$ for different values of Reynolds number. In this figure, x axis indicates vessel lenght (m), y axis lumen diameter (m), and the colorbar indicates velocity magnitudes (m/s).

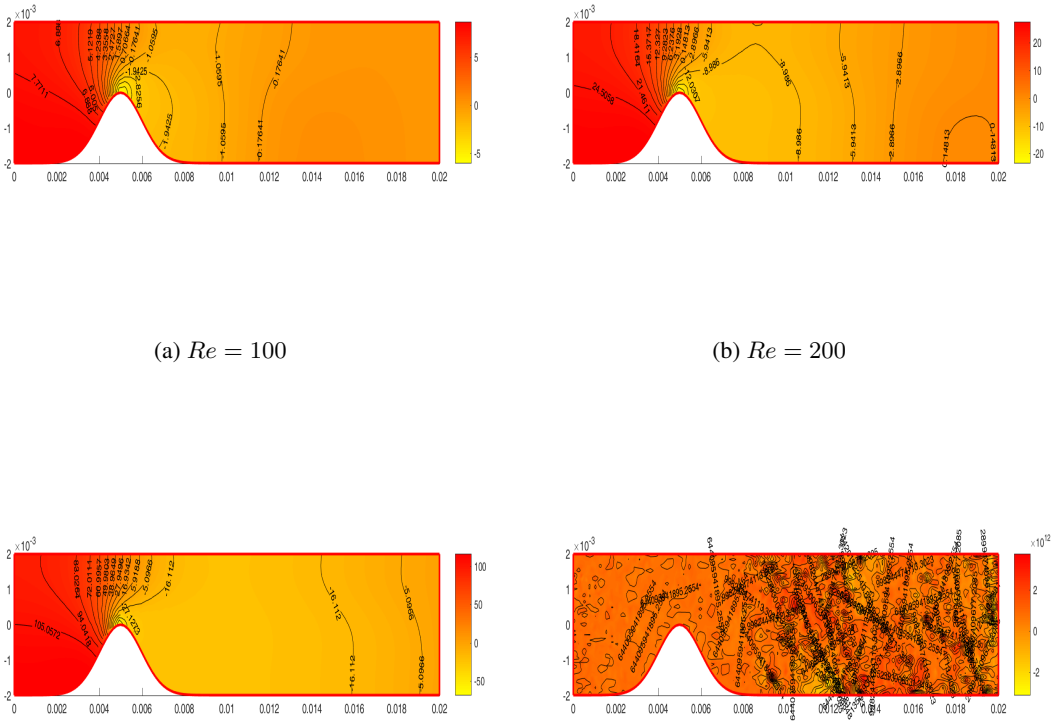

(a) $Re = 100$ (b) $Re = 200$

(c) $Re = 400$ (d) $Re = 600$

Figure 7.2: Pressure profiles for $\gamma = 1$ for different values of Reynolds number. In this figure, x axis indicates vessel lenght (m), y axis lumen diameter (m), and the colorbar indicates pressure values (Pa).

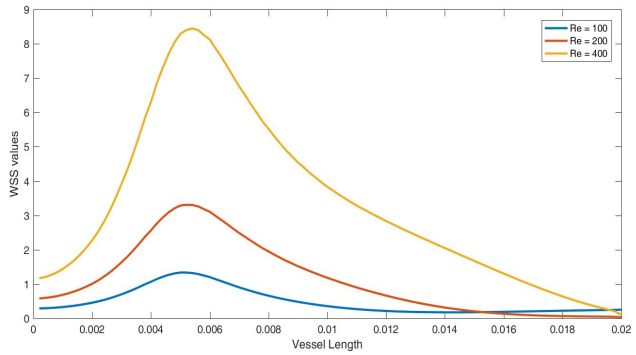

(a) Upper Wall

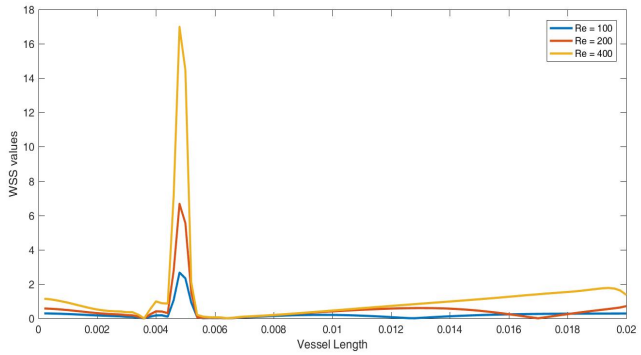

(b) Bottom Wall

Figure 7.3: WSS values for $\gamma = 1$ for different values of Reynolds number. In this figure, x axis indicates vessel length (m) and y axis indicates WSS values (Pa).

Table 7.1: Maximum and minimum WSS (Pa) values for Figure 7.3

	$Re = 100$	$Re = 200$	$Re = 400$
Upper Wall			
Maximum WSS (Pa)	1.3355	3.3093	8.4466
Minimum WSS (Pa)	0.1758	0.0312	0.1041
bottom wall			
Maximum WSS (Pa)	2.6666	6.6767	16.9900
Minimum WSS (Pa)	0.0047	0.0042	0.0062

- The tests are conducted for $Re = 100, 200, 400, 600, 1000$ and 1200. For Reynolds number more than 400, we cannot get meaningful results and observe lack of convergence of the results. Sudden expansion of stenosis is known to be a hard geometry to solve, and lack of convergence usually occur. Therefore a suitable stabilization is needed.

- From Figure 7.11, 7.1b and 7.1c, it is observed that, maximum flow velocity increases abruptly just before and around the stenosis, this increased part of the velocity field is sometimes called a flow jet.

- The velocity magnitude increases with increasing Reynolds number, and back flow occurs close to the wall after the stenosis. In addition to that, a recirculation region occurs right after the constriction. With increasing Reynolds number, the flow jet increases and its angle with longitudinal axis decreases, therefore the recirculation region expands. It is observed in Figure 7.3b that, just after the recirculation, there exists a stagnant point where WSS is 0. This point corresponds to the point there the recirculation ends.

- Redevelopment of the flow should be described as restoring of the flow to its initial state. From velocity magnitude and WSS plots we can see that the redevelopment length is the smallest for $Re = 100$, and it increases with increasing Reynolds number.

- In Figure 7.2a, 7.2b and 7.2c, it is observed that the amplitude of the pressure field increases remarkably with increasing Reynolds number. Pressure decreases significantly at narrow region due to the sudden increase in the velocity magnitude. The decrease gets higher with increasing Reynolds Number, and focal (focus center) points occur in the pressure field due to pressure drop. It is stated in [44] that this pressure drop would lead the stenosis tempted to get even narrower.

- The magnitudes of pressure drops are not linearly dependent on Reynolds number and the inlet velocity. Before stenosis, the pressure is significantly high. After the abrupt drop at the constriction, it increases slowly through the outlet.

- We can see from Figure 7.3a and 7.3b and Table 7.1 that, WSS increases with increasing Reynolds number. At constriction regions it demonstrates an in-

crease since the constriction reroutes the flow through the upper wall. This leads an increased friction, and WSS values reaches up to 8.4466 Pa for $Re = 400$ at the upper wall.

- As for the bottom wall with stenosis, the WSS shows a first increase due to the first contact of the flow. After that it shows an enormous increase at the constriction, reaches up to 16.99 Pa for $Re = 400$, decreases to around zero through the stagnant point. After the stagnant point, it gets stabilized to its natural value.
- With increasing Reynolds number, WSS values increases almost linearly.
- For the upper wall, the stenosis leads the flow through the upper wall and the friction at the upper wall in that region increases, and WSS also increases.
- The results are consistent with [44].

7.1.1.1 Effect of Stabilization

For $Re = 600$, we are unable to get meaningful results without stabilization, due to the lack of convergence of the results caused by the stenosis geometry. But with $\gamma = 10000$, the methods gives meaningful results.

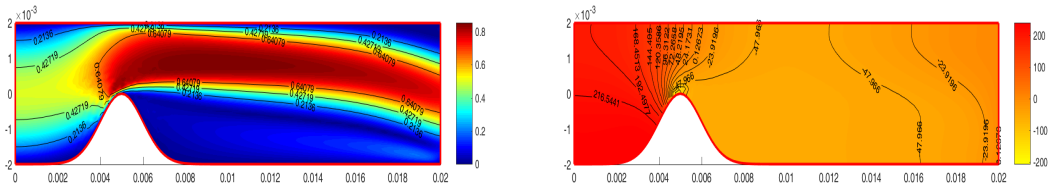

(a) Velocity magnitude for $\gamma = 10000$ and $Re = 600$ (b) Pressure profile for $\gamma = 10000$ and $Re = 600$

Figure 7.4: $\gamma = 10000$ and $Re = 600$. The axis x indicates vessel length (m), y axis lumen diameter (m), the colorbar in (a) indicates velocity magnitudes (m/s), and (b) indicates pressure values (Pa).

Using the results, with increasing Reynolds number we can again validate that,

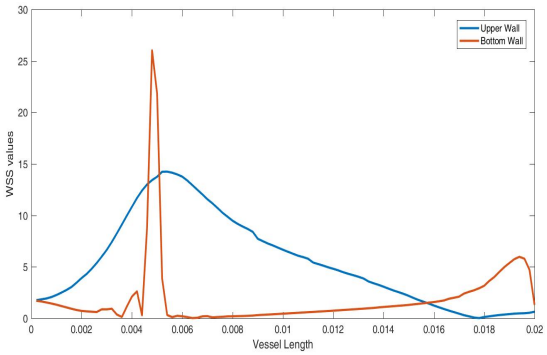

Figure 7.5: WSS values for $\gamma = 10000$ and $Re = 600$. In this figure, x axis indicates vessel length (m) and y axis indicates WSS values (Pa).

Table 7.2: Maximum and minimum WSS values (Pa) for Figure 7.5

	$Re = 600$
upper wall	
maximum WSS (Pa)	14.2500
minimum WSS (Pa)	0.0272
bottom wall	
maximum WSS (Pa)	26.0317
minimum WSS (Pa)	0.0286

- From Figure 7.4a, we can see that the velocity magnitude increases.
- The flow jet region increases and its angle with longitudinal axis decreases, therefore the recirculation region expands.
- Recirculation region and redevelopment length increases.
- From Figure 7.4b, we can see that the pressure field amplitude increases remarkably. Pressure drops are observed again, just as expected.
- From Figure 7.5 and Table 7.2 we can see that WSS increases around the constriction at the upper wall, and reaches up to 14.25 Pa, and at the bottom wall it reaches up to 26.0317 Pa.

7.1.2 Shifted Stenosis

Since a symmetric stenosis is not always the case, a small shift between two constrictions are considered to show the effect of asymmetry in a stenosis problem in [44]. We have investigated a more remarkable shift, and introduced a more detailed investigation on velocity magnitudes and pressure profiles, together with WSS values.

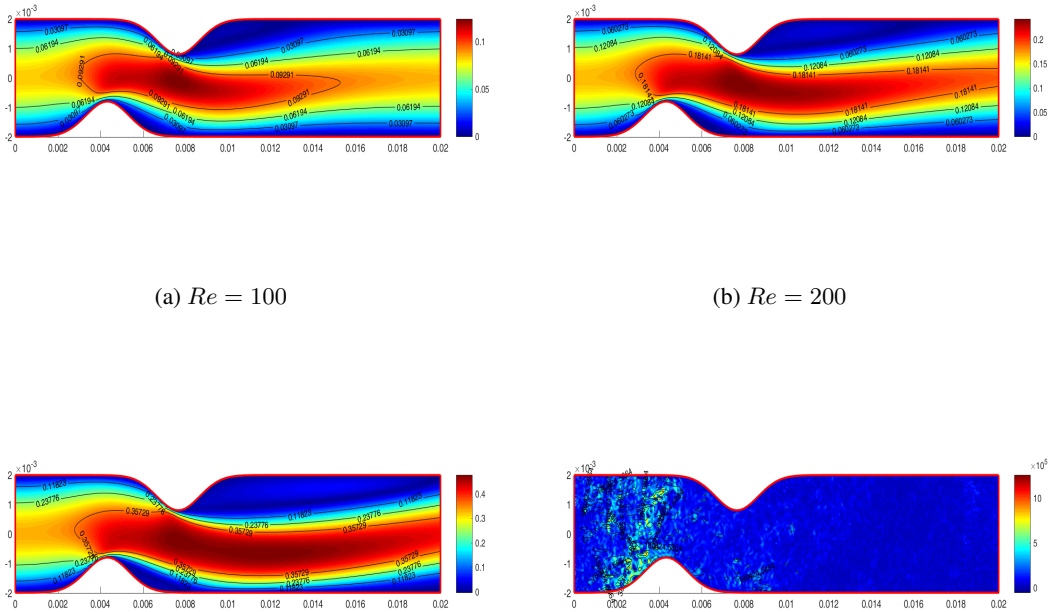

(a) $Re = 100$

(b) $Re = 200$

(c) $Re = 400$

(d) $Re = 600$

Figure 7.6: Velocity magnitudes for $\gamma = 1$ for different values of Reynolds number. In this figure, x axis indicates vessel lenght (m), y axis lumen diameter (m), and the colorbar indicates velocity magnitudes (m/s).

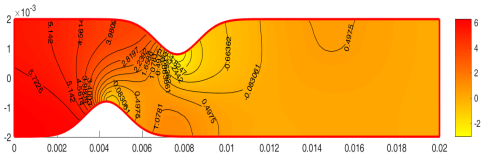

(a) $Re = 100$

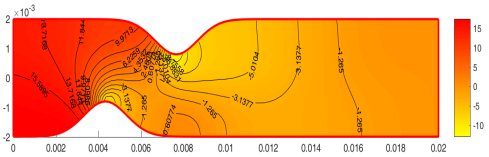

(b) $Re = 200$

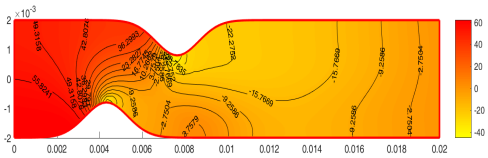

(c) Pressure values for $\gamma = 1$ and $Re = 400$

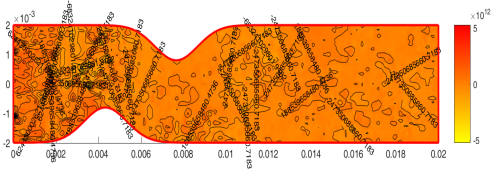

(d) $Re = 600$

Figure 7.7: Pressure profiles for $\gamma = 1$ for different values of Reynolds number. In this figure, x axis indicates vessel lenght (m), y axis lumen diameter (m), and the colorbar indicates pressure values (Pa).

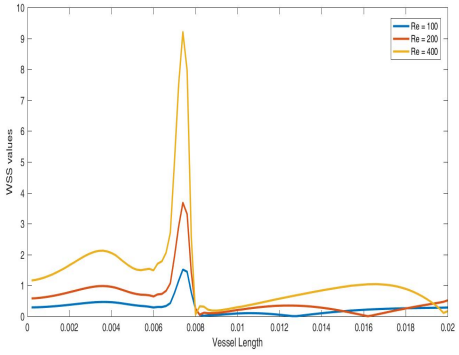

(a) Upper Wall

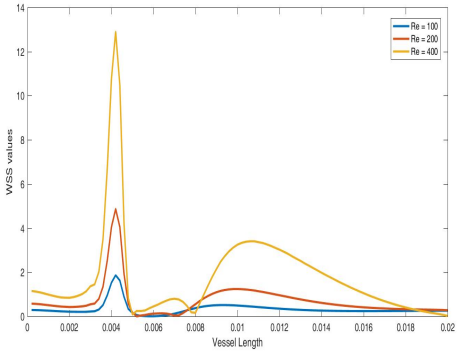

(b) Bottom Wall

Figure 7.8: WSS values for $\gamma = 1$ for different values of Reynolds number. In this figure, x axis indicates vessel length (m) and y axis indicates WSS values (Pa).

Table 7.3: Maximum and minimum WSS values (Pa) for Figure 7.8

	$Re = 100$	$Re = 200$	$Re = 400$
upper wall			
maximum WSS (Pa)	1.5164	3.6773	9.2063
minimum WSS (Pa)	0.0066	0.0051	0.0576
bottom wall			
maximum WSS (Pa)	1.8642	4.8646	12.8926
minimum WSS (Pa)	0.0039	0	0.0161

- The tests are conducted for $Re = 100, 200, 400, 600, 1000$ and 1200.
- From Figure 7.6a, 7.6b and 7.6c, it is observed that flow jet follows more complex path. Right after the constriction in the upper wall, a recirculation (vortex) occurs, this can also be validated from the WSS plot in Figure 7.8a.
- Right after the constriction in the bottom wall, an apparent recirculation occurs for $Re > 200$. This can also be observed from the stagnant point on WSS plot in Figure 7.8b.
- Right after the constriction in the upper wall, an apparent recirculation occurs for all the cases. This can also be observed from the stagnant point on WSS plot on Figure 7.8b.
- Similar with problem in Section 7.1.1, velocity magnitude and length of the flow jet increase, angle of the jet flow with longitudinal axis decrease, recirculation region in both walls expands and redevelopment length increases with increasing Reynolds number.
- From Figure 7.7a, 7.7b and 7.7c, we can again see that the pressure field amplitude increases remarkably with increasing Reynolds number. Pressure decreases significantly at narrow region, and the decrease gets higher with increasing Reynolds Number. A higher drop occurs in the second stenosis, and focal pressure points are observed in the pressure map on the both stenosis due to pressure drops. The magnitudes of pressure drops seem not to be linearly

dependent on inlet flow and the Reynolds number.

- Similar with first problem, pressure is significantly high before both of the stenosis constrictions.
- WSS values increases linearly with increasing Reynolds number. It is given in Table 7.3 that, it reaches up to $9.2063Pa$ at the upper wall, and $12.8926Pa$ at the bottom wall for $Re = 400$.

7.1.3 Different Rates Of Stenosis

Effect of rate of stenosis is studied in [44], as well as [45] and [46]. In [45], the rate of stenosis studied with different hemodynamic features such as WSS, time averaged wall shear stress gradient (TAWSSG) and oscillatory shear index (OSI), with assumption that blood is non-Newtonian. In [46], the rate of stenosis is studied in curved vessels with steady and pulsatile flow with a constant viscosity using WSS distributions along the vessel. In [44], velocity and pressure profiles for limited number of different rates are studied with steady Navier-Stokes equations with a constant viscosity. In this problem we investigate a stenosis of rates of %25, %50 and %75 with grad-div stabilized steady Navier-Stokes equations, using the geometry from [44].

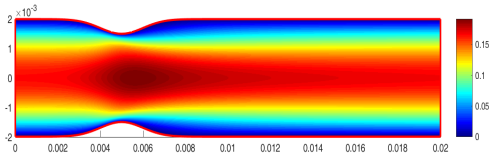

(a) %25 Stenosis

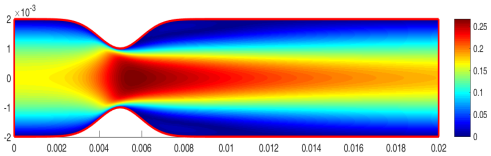

(b) %50 Stenosis

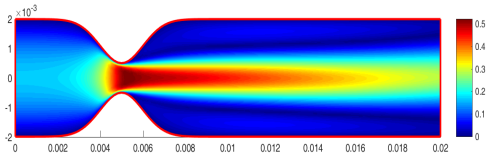

(c) %75 Stenosis

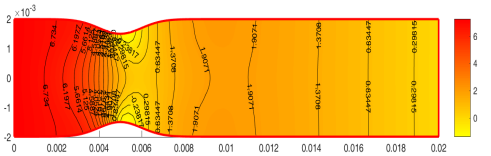

(d) %25 Stenosis

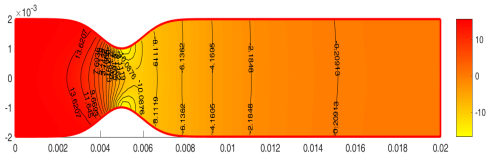

(e) %50 Stenosis

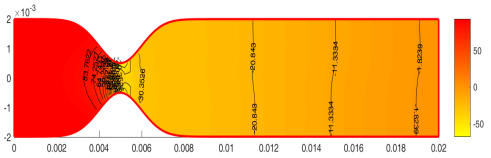

(f) %75 Stenosis

Figure 7.9: Velocity magnitudes for $\gamma = 1$ and $Re = 200$ for different rates of stenosis. In this figure, x axis indicates vessel lenght (m), y axis lumen diameter (m), and the colorbar in a, b and c indicates velocity magnitudes (m/s), d, e and f indicates pressure values (Pa).

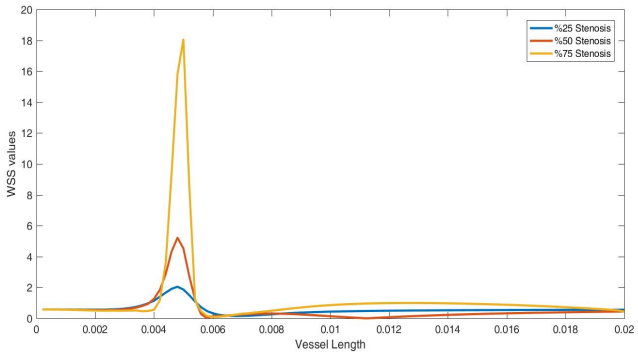

(a) Upper wall for different rates of stenosis

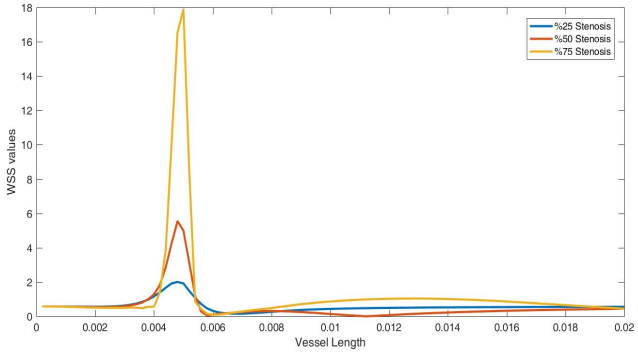

(b) Lower wall for different rates of stenosis

Figure 7.10: WSS values for $\gamma = 1$ and $Re = 200$ for different rates of stenosis

Table 7.4: Maximum and minimum WSS values (Pa) for Figure 7.10

	%25 Stenosis	%50 Stenosis	%75 Stenosis
upper wall			
maximum WSS (Pa)	2.0451	5.2211	18.0553
minimum WSS (Pa)	0.1490	0.0030	-0.0330
bottom wall			
maximum WSS (Pa)	2.0039	5.5439	17.8878
minimum WSS (Pa)	0.1532	0.0038	0.1006

- It is observed from Figure 7.9a, 7.9b and 7.9c that, velocity magnitude increases with increased rate of stenosis.

- Maximum velocity (flow jet) becomes apparent for stenosis rate of %50 and more, and gets higher in magnitude as stenosis gets more severe. In case of higher stenosis rate the length of the jet gets smaller.

- It is observed from Figure 7.9d, 7.9e and 7.9f that, pressure before the stenosis increases enormously with increasing rate of stenosis. With increased velocity magnitude at constriction, pressure drops significantly, and focal pressure points occur in both sides.

- It is observed from Figure 7.10a, 7.10b that, WSS increases at the constriction region significantly. The maximum WSS increases as the rate of stenosis increases. In Table 7.4, maximum WSS value of 18.0553 Pa is observed for %75 rate of stenosis.

7.1.3.1 Effect of Stabilization

Without stabilization, we cannot obtain meaningful numerical results for a stenosis rate of more than %75. In the figures, we can see the velocity, pressure and WSS distribution for a rate of %85 stenosis.

Table 7.5: Maximum and minimum WSS values (Pa) of the case $Re = 600$ for Figure 7.11

upper wall	
maximum WSS (Pa)	46.4068
minimum WSS (Pa)	-0.0330
bottom wall	
maximum WSS (Pa)	42.2058
minimum WSS (Pa)	0.0177

While we can make same comments for increasing rate of stenosis, here we can see an asymmetry in the velocity, pressure and WSS distributions. If we look at first

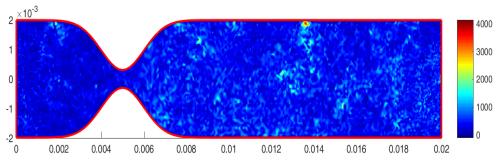

(a) Velocity magnitude for $\%85$ Stenosis with $\gamma = 0$

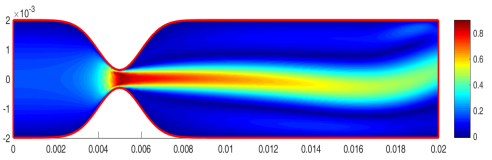

(b) Velocity magnitude for $\%85$ Stenosis with $\gamma = 1$

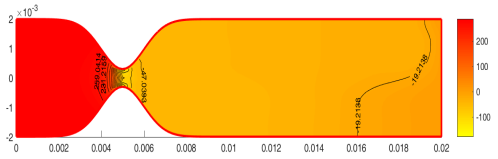

(c) Pressure profile for $\%85$ Stenosis with $\gamma = 1$

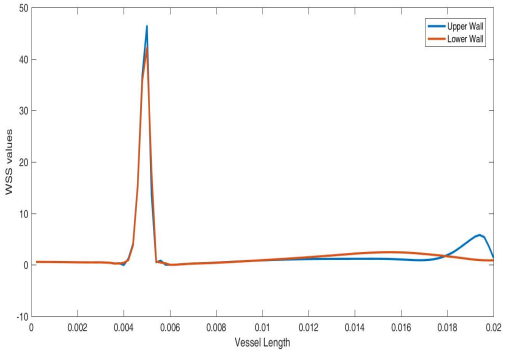

(d) WSS values for $\%85$ Stenosis with $\gamma = 1$

Figure 7.11: Effect of stabilization for $\%85$ rate of stenosis.

half length of the vessel, the asymmetry is not observable, but for the remaining half, asymmetry is visible and expands through the outlet. This is probably caused by the contribution of the grad-div term and propagates as the length increases. Other than that, one can observe that;

- From Figure 7.11a, we can see that the method does not give meaningful results without any stabilization.
- From Figure 7.11b, we can see that the velocity magnitude increases with increasing stenosis severity.
- Maximum velocity (flow jet) gets higher for higher stenosis severities, but the length of the jet gets smaller for higher stenosis severities.
- From Figure 7.11c, we can see that the pressure before the stenosis increases dramatically with increasing rate of stenosis.

7.1.4 Saccular Aneurysm

In [47], a fusiform aneurysm is studied with Navier-Stokes equations with both Newtonian and non-Newtonian behavior of the blood. To investigate the effect of aneurysm on flow patterns, different hemodynamic features such as WSS, time averaged wall shear stress gradient (TAWSSG) and oscillatory shear index (OSI) are considered. In [48], WSS and velocity fields are used to investigate the flow patterns on a fusiform aneurysm, assuming the blood is Newtonian. For problem 4 and 5, we have inspired from this two studies, and obtained the geometry with some variations from the geometry given in [44].

Table 7.6: Maximum and minimum WSS values (Pa) for Figure 7.14

	$Re = 100$	$Re = 200$	$Re = 400$	$Re = 600$	$Re = 1000$	$Re = 1200$
Upper Wall						
Maximum WSS (Pa)	0.3019	0.6082	1.2184	1.8269	3.0388	3.6437
Minimum WSS (Pa)	0.2461	0.5005	1.0205	1.5484	2.6170	3.1553
Bottom Wall						
Maximum WSS (Pa)	0.4379	0.9072	1.8477	2.7746	4.6341	5.5643
Minimum WSS (Pa)	0.0013	0.0048	0.0099	0.0270	0.0622	0.0706

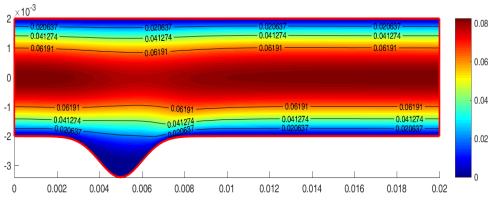

(a) $Re = 100$

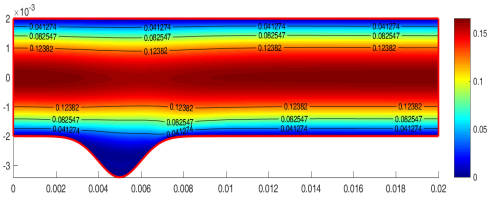

(b) $Re = 200$

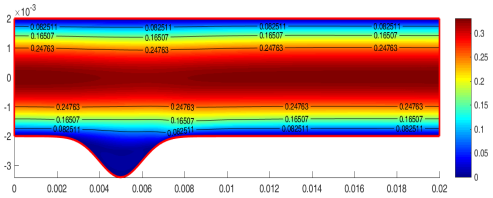

(c) $Re = 400$

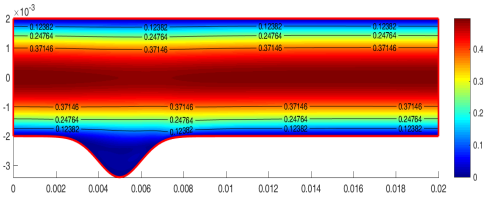

(d) $Re = 600$

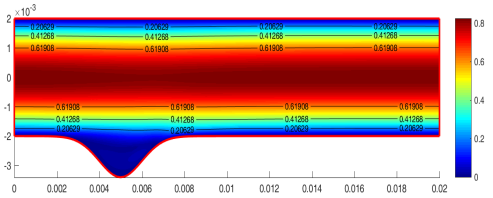

(e) $Re = 1000$

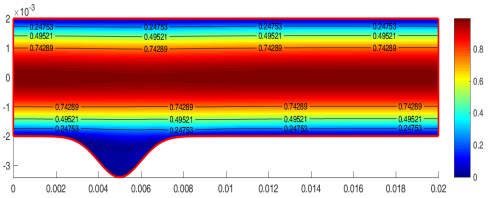

(f) $Re = 1200$

Figure 7.12: Velocity magnitudes for $\gamma = 1$ for different values of Reynolds number. In this figure, x axis indicates vessel lenght (m), y axis lumen diameter (m), and the colorbar indicates velocity magnitudes (m/s).

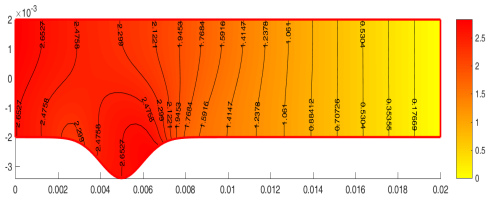

(a) $Re = 100$

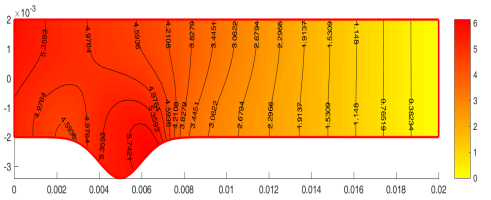

(b) $Re = 200$

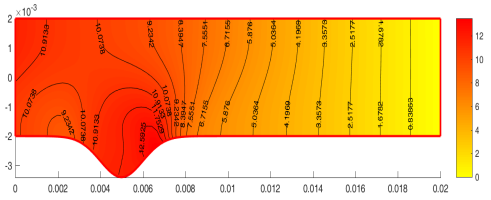

(c) $Re = 400$

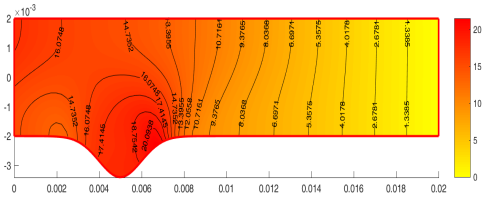

(d) $Re = 600$

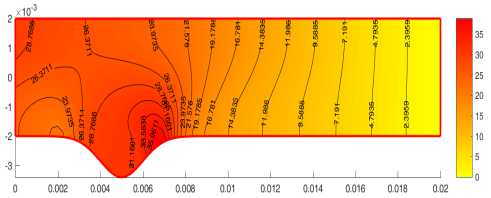

(e) $Re = 1000$

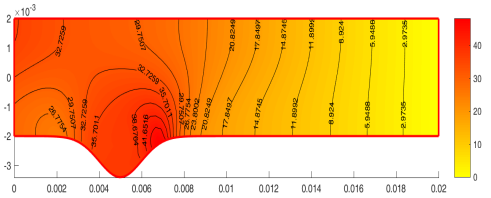

(f) $Re = 1200$

Figure 7.13: Pressure profiles for $\gamma = 1$ for different values of Reynolds number. In this figure, x axis indicates vessel lenght (m), y axis lumen diameter (m), and the colorbar indicates pressure values (Pa).

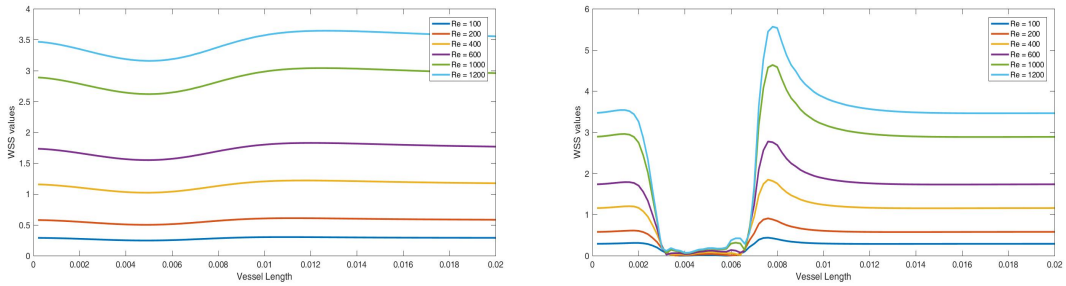

(a) Upper Wall

(b) Lower Wall

Figure 7.14: Wall shear stress values for $\gamma = 1$ for different values of Re. In this figure, x axis indicates vessel length (m) and y axis indicates WSS values (Pa).

- The tests are conducted for $Re = 100, 200, 400, 600, 1000$ and 1200. This geometry is less complex than the stenosis type, therefore we have been able to reach $Re = 1200$ in the experiments.
- In Figure 7.12a to 7.12f, one can see that the velocity magnitude increases with increasing Reynolds number.
- Recirculation region occurs in the aneurysm region, this can be understood from WSS plot in Figure 7.14b.
- In Figure 7.13a to 7.13f, one can see that, the pressure field amplitude increases remarkably with increasing Reynolds number. Pressure is significantly higher at expanded region, and it gets higher with increasing Reynolds Number.
- In Figure 7.12a, 7.12b and Table 7.6, one can see that WSS at upper wall decreased with the effect of aneurysm dilation. This means a disturbance in the endothelial line-up and will result with a cardiovascular dysfunction [49].
- Two focal pressure centers in the pressure field occurs at the beginning and end of the aneurysm.
- With increasing Reynolds number, the focal pressure centers at the end of aneurysm becomes more visible.
- For the bottom wall Figure 7.14b indicates that, WSS is decreased at the aneurysm region. The friction and WSS shows a fast increase, then goes to stable state.

7.1.5 Asymmetric Fusiform Aneurysm

This is a fusiform aneurysm with different lengths of dilation along both sides, and similar studies were presented in the introduction of Section 7.1.4. In this study, we aimed to investigate the flow patterns in a fusiform aneurysm, as well as the effect of asymmetric dilation on flow patterns. This geometry is obtained with some variations on the geometry from [44], and is not studied in this paper.

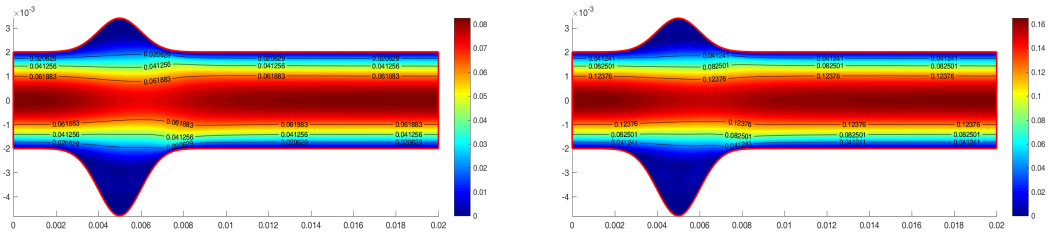

(a) $Re = 100$

(b) $Re = 200$

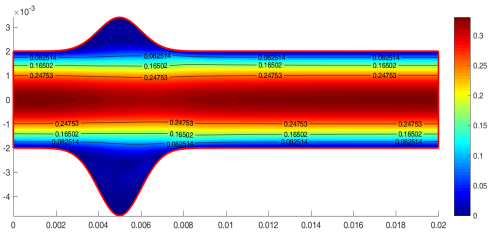

(c) $Re = 400$

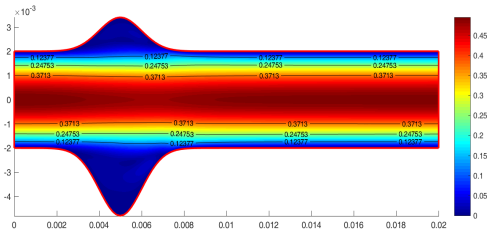

(d) $Re = 600$

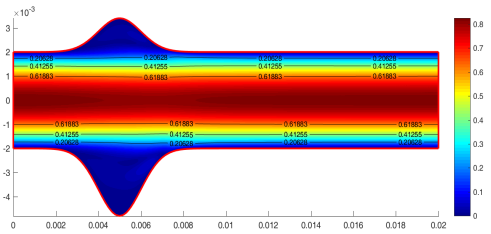

(e) $Re = 1000$

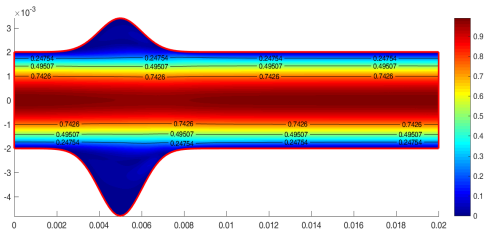

(f) $Re = 1200$

Figure 7.15: Velocity magnitudes for $\gamma = 1$ for different values of Reynolds number. In this figure, x axis indicates vessel lenght (m), y axis lumen diameter (m), and the colorbar indicates velocity magnitudes (m/s).

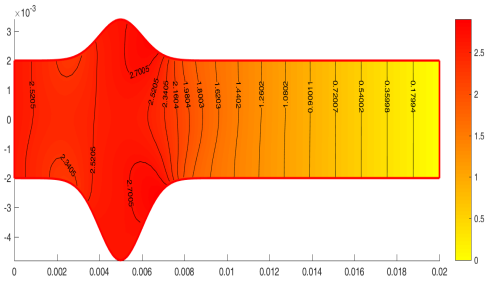

(a) $Re = 100$

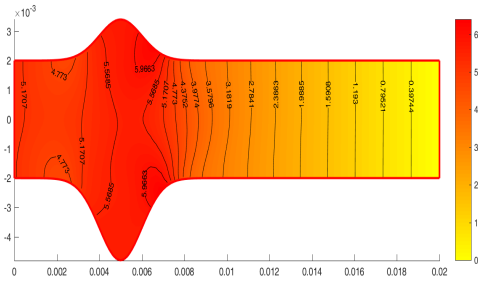

(b) $Re = 200$

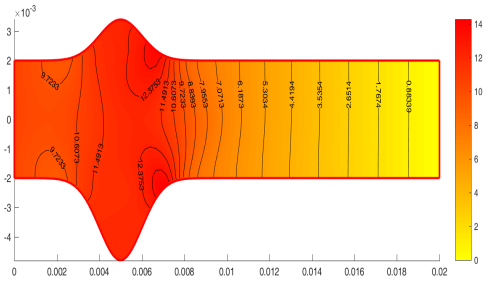

(c) $Re = 400$

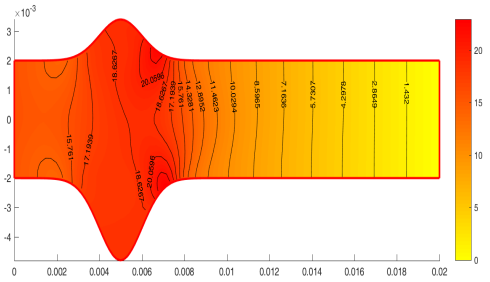

(d) $Re = 600$

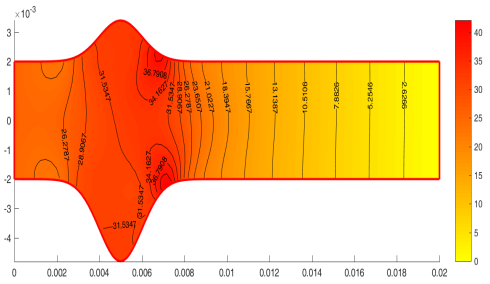

(e) $Re = 1000$

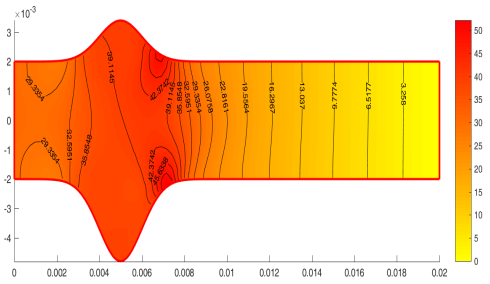

(f) $Re = 1200$

Figure 7.16: Pressure profiles for $\gamma = 1$ for different values of Reynolds number. In this figure, x axis indicates vessel lenght (m), y axis lumen diameter (m), and the colorbar indicates pressure values (Pa).

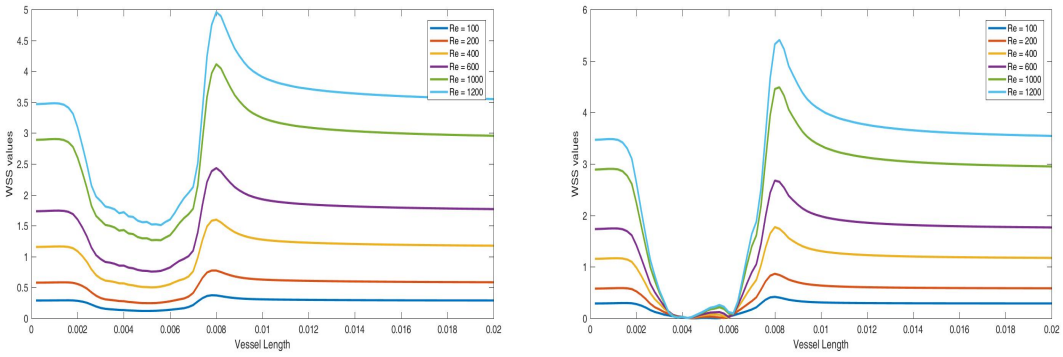

(a) Upper Wall

(b) Lower Wall

Figure 7.17: WSS values for $\gamma = 1$ for different values of Reynolds number. In this figure, x axis indicates vessel length (m) and y axis indicates WSS values (Pa).

Table 7.7: Maximum and minimum WSS values (Pa) for Figure 7.17

	$Re = 100$	$Re = 200$	$Re = 400$	$Re = 600$	$Re = 1000$	$Re = 1200$
Upper Wall						
Maximum WSS (Pa)	0.3739	0.7741	1.5980	2.4332	4.1150	4.9564
Minimum WSS (Pa)	0.1198	0.2459	0.5017	0.7577	1.2687	1.5146
bottom wall						
Maximum WSS (Pa)	0.4172	0.8661	1.7721	2.6758	4.4892	5.4082
Minimum WSS (Pa)	0.0018	0.0052	0.0096	0.0091	0.0073	0.0067

- From Figure 7.15a to 7.15f, we can see that the velocity magnitude increases with increasing Reynolds number.
- Weak recirculation regions occurs in the aneurysm region, this can be validated from Figures 7.17a and 7.17b.
- The flow goes to redevelopment state very fast.
- From Figure 7.16a to 7.16f, we observe that the amplitude of the pressure field increases remarkably with increasing Reynolds number.
- Pressure increases significantly at expanded regions, and the decrease gets higher with increasing Reynolds Number. The pressure at the more expanded region is slightly higher than the upper aneurysm.

- Four focal points in the pressure field occurs at the beginning and end of both of the aneurysm, and it gets visible with increasing Reynolds number.
- From Figure 7.16a, 7.16b and 7.7, we can see that the bottom line is exposed to higher WSS.
- WSS values increases linearly with increasing Reynolds number.

7.2 Time-Dependent Navier Stokes Equations

In this section, time dependent Navier-Stokes equations

$$\begin{aligned} u_t + (u \cdot \nabla)u - \nu\Delta u + \nabla p = f, \quad in \quad (0,T] \times \Omega \\ \nabla \cdot u = 0 \quad in \quad (0,T] \times \Omega \\ u(x,0) = u_0(x) \quad for \quad x \in \Omega \\ u = 0 \quad on \quad \Gamma_{Wall} \\ n \cdot \sigma = 0 \quad on \quad \Gamma_{out} \\ u = c \quad on \quad \Gamma_{in}. \end{aligned} \tag{7.2}$$

were implemented using grad-div stabilized Backward Euler fully discrete scheme. In the remaining sections, applications of time dependent Navier-Stokes equations are introduced. In Section 7.2.1, we introduce an asymmetric branching artery. The expection in this problem is to observe a drop in wall shear stress values through the branch, and a stabilization through the outlet. In Section 7.3.1, a branching geometry together with an aneurysm (Cerebral Aneurysm) is introduced. The expectation here is to observe lower velocity magnitudes and higher pressure values at the aneurysm. Since periodic boundary conditions are used here, another expectation is to observe velocity magnitudes to be maximum at the systolic phase, and minimum at the diastolic phase. Finally in Section 7.3.2, we introduce a symmetric branching artery. The expectation in this problem is to observe smaller wall shear stress values around the branching region and a stabilization through the outlet. Again, due to the periodic

boundary conditions, observing maximum velocity magnitudes at the systolic phase, and minimum at the diastolic phase is another expectation in this problem.

7.2.1 Asymmetric Branching Artery

Arteries spread through the whole body with branches and this system is sometimes called as arterial tree. Even though plaque formation has major causes such as obesity and malnutrition, the plaque mostly forms in particular places in the artery. Atherosclerosis occurs in branching regions of the artery, in general [50]. Therefore, investigation of branches is an important problem of cardiovascular modelling. Geometry of branching arteries should be classified as asymmetric branches, such as in [51] and [52], and symmetric branches such as in [4]. In this geometry, we have inspired from [51], by picking 24 mm of main vessel diameter and 14 mm of branching vessel diameter and a 45 degree angle with longitudinal axis. We have implemented the geometry by ourselves and the codes are given at the end of the thesis.

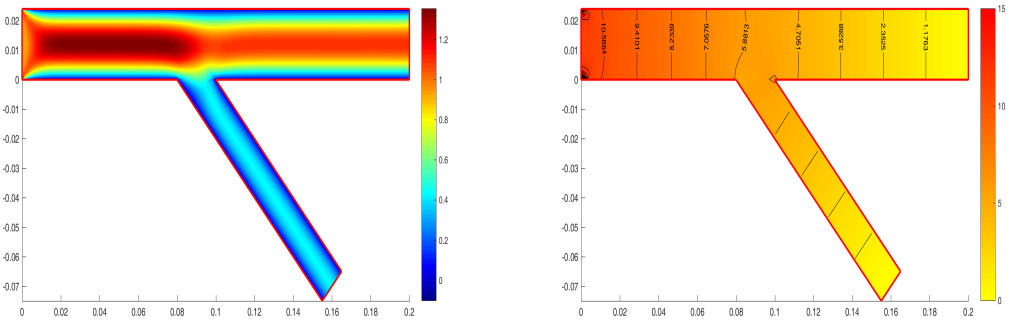

(a) Velocity magnitude for $\gamma = 1$,$Re = 820$

(b) Pressure field for $\gamma = 1$,$Re = 820$

Figure 7.18: Velocity and pressure values for $\gamma = 1$. In this figure, x axis indicates vessel lenght (m), y axis lumen diameter (m), the colorbar a indicates velocity magnitudes (m/s), and the colorbar b indicates pressure values (Pa).

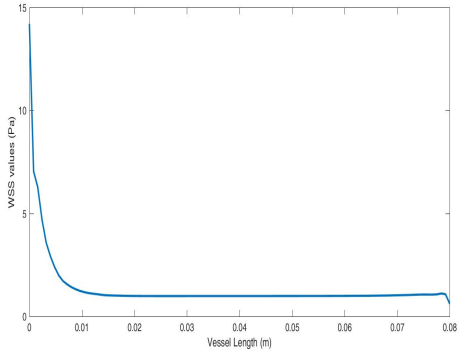

(a) WSS values at wall A

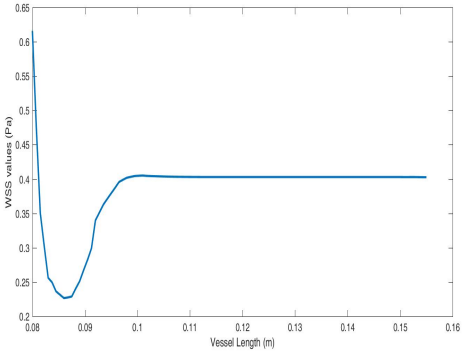

(b) WSS values at wall B

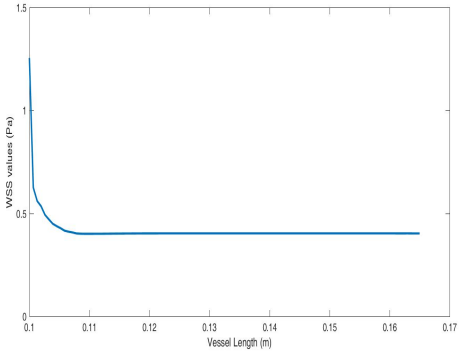

(c) WSS values at wall C

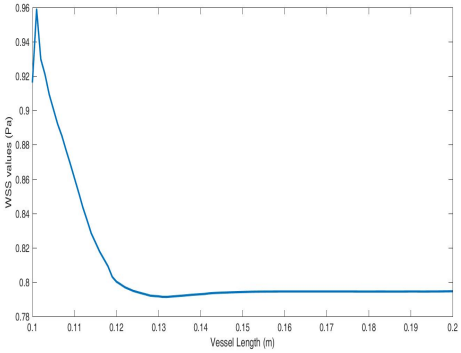

(d) WSS values at wall D

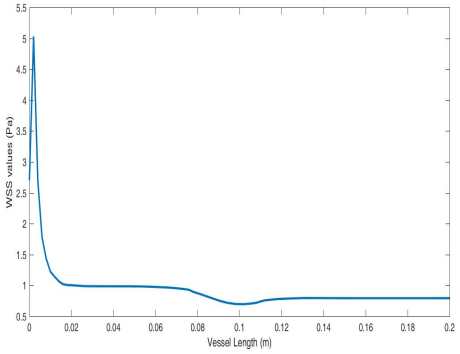

(e) WSS values at wall E

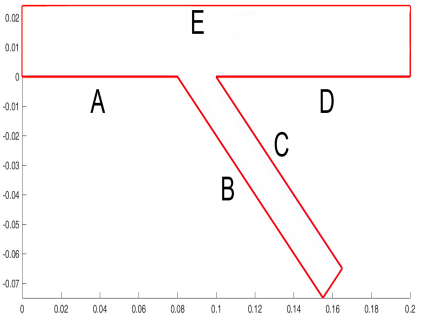

(f) The geometry and labelling of walls

Figure 7.19: WSS values for $Re = 820$ and $\gamma = 1$

- Observing from Figure 7.18a, it takes time for flow to develop due to the inlet velocity profile. After it is developed, the regions close to the boundary forms a boundary layer to adapt the no slip boundary condition.
- After the branch, the maximum velocity at the main vessel decreases through the outlet, since some part of the flow goes through the branching vessel.

- Observing from Figure 7.18b, we can say that the pressure decreases through the outlet.
- Observing from Figure 7.19a, we can see that the WSS is decreased to a stabilized level until the flow is fully developed. After development, it becomes stable through the branching region.
- Observing from Figure 7.19b, the flow first rerouted through the wall C, and the stabilization length of B is higher than of C.
- Observing from Figure 7.19c, after the flow routes to the intersection of C and D, it gets decreased and stabilized through the outlet.
- Observing from Figure 7.19d, WSS increases significantly and stabilizes through the outlet after the branch at wall D.
- Observing from Figure 7.19e, we can see that the WSS is decreased to a stabilized level until the flow fully developed. At the branching region it shows a remarkable decrease and stabilized after the branching region. This decrease around the branching region causes continually low WSS values, therefore this part of the branch is susceptible to plaque formation.

7.3 Pulsating Flow

To simulate more realistic flow, we have used the boundary conditions from the study [1],

$$n \cdot \sigma = 0 \quad on \quad \Gamma_{out}$$

$$u = Asin^2(wt) \quad on \quad \Gamma_{in}$$

which is a time dependent periodic boundary condition, a period represents one cardiac cycle. For the following experiments, we have introduced four different subimages for velocity, pressure and WSS profiles, each representing different phases of cardiac cycle each representing $\frac{1}{4}$ cardiac cycle ahead of the previous.

7.3.1 Cerebral Aneurysm

This geometry is given in [44] and no comments were introduced on the results. This is a saccular aneurysm, occured in cerebral artery in the brain, therefore called as cerebral aneurysm.

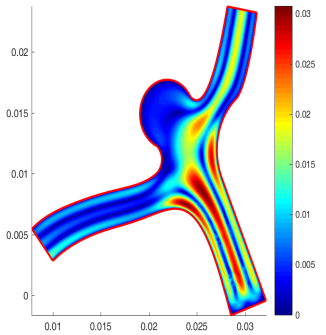

(a) Velocity magnitude for $\gamma = 1$, $Re = 200$ at approximately $1/4$ of cardiac cycle

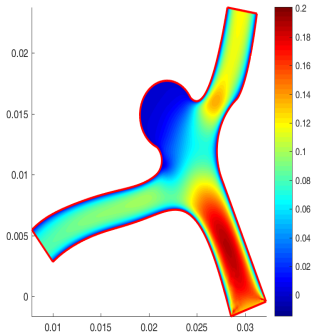

(b) Velocity magnitude for $\gamma = 1$, $Re = 200$ at approximately $2/4$ of cardiac cycle

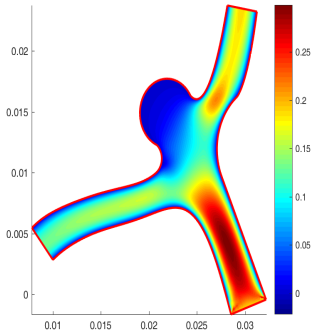

(c) Velocity magnitude for $\gamma = 1$, $Re = 200$ at approximately $3/4$ of cardiac cycle

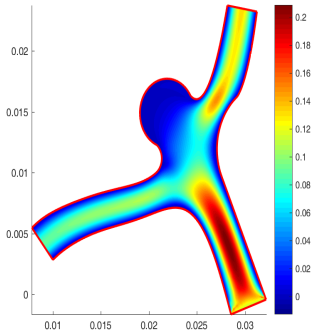

(d) Velocity magnitude for $\gamma = 1$, $Re = 200$ at approximately $4/4$ of cardiac cycle

Figure 7.20: Velocity magnitudes for $\gamma = 1$ for different phases of cardiac cycle. In this figure, x and y axes indicates vessel lenght (m), and the colorbar indicates velocity magnitudes (m/s).

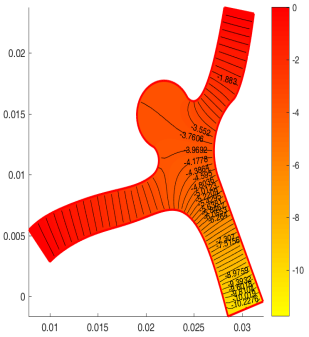

(a) Pressure profile for $\gamma = 1$, $Re = 200$ at approximately $1/4$ of cardiac cycle

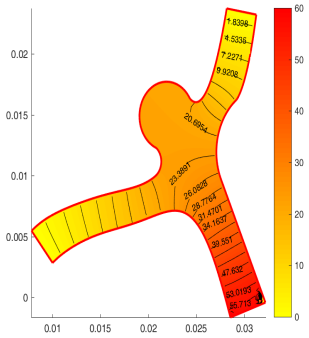

(b) Pressure profile for $\gamma = 1$, $Re = 200$ at approximately $2/4$ of cardiac cycle

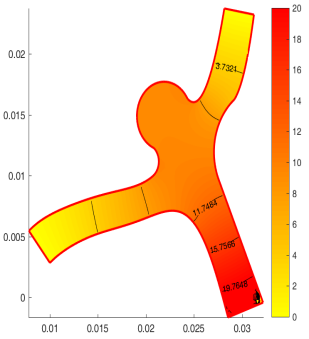

(c) Pressure profile for $\gamma = 1$, $Re = 200$ at approximately $3/4$ of cardiac cycle

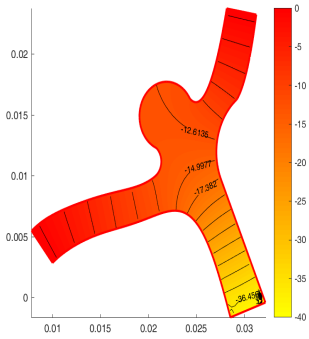

(d) Pressure profile for $\gamma = 1$, $Re = 200$ at approximately $4/4$ of cardiac cycle.

Figure 7.21: Pressure profiles for $\gamma = 1$ for different phases of cardiac cycle. In this figure, x and y axes indicates vessel lenght (m), and the colorbar indicates pressure values (Pa).

- Figure 7.20c and 7.21c represent the beginning of the systole. In that phase, maximum velocity at the inlet occurs due to the contraction of the ventricles. Figure 7.20a and Figure 7.21c represent the beginning of diastole. In this phase, minimum velocity at the inlet occurs since ventricles are relaxed.
- One can observe from Figure 7.20a that, backflow occurs at the end of systole.
- One can observe from Figure 7.20c, velocity field and maximum velocity is much higher at the beginning of the systole due to the contraction of the ventricles, and high flow rate is apparent through the inlet.
- One can observe from 7.20a that, vortex occurs in the aneurysm region at the end of systole.

- The pressure at the cerebral aneurysm is higher then its surrounding.
- One can observe from Figure 7.20a that, once the velocity becomes zero, back flow and vortex occurs due to the energy in the system. As the flow continues through the systolic phase, the energy is distributed inside, and this yields regular flows, seen in Figure 7.20b, 7.20c and 7.20d.

7.3.2 Symmetric Branching Artery

In Section 7.2.1, we have introduced an asymmetric branching artery. Symmetric branches, as well as asymmetric ones, are also concern of literature, e.g. [4]. In this problem we introduce a symmetric branch of vessels, introduce their velocity magnitudes and pressure values, together with WSS values, to investigate their patterns in different phases of cardiac cycle.

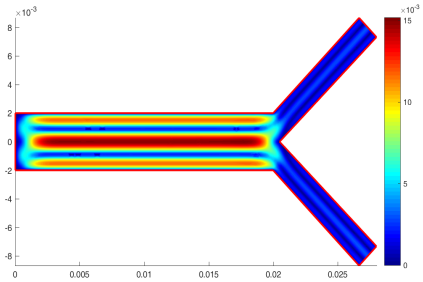

(a) Velocity magnitude for $\gamma = 1$, $Re = 200$ at approximately $1/4$ of cardiac cycle

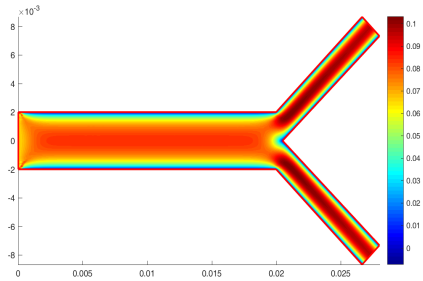

(b) Velocity magnitude for $\gamma = 1$, $Re = 200$ at approximately $2/4$ of cardiac cycle

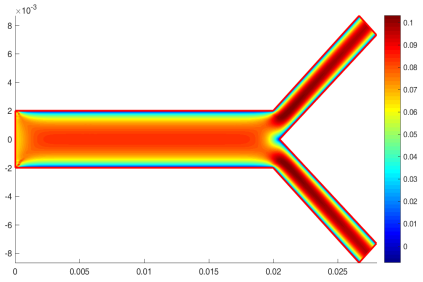

(c) Velocity magnitude for $\gamma = 1$, $Re = 200$ at approximately $3/4$ of cardiac cycle

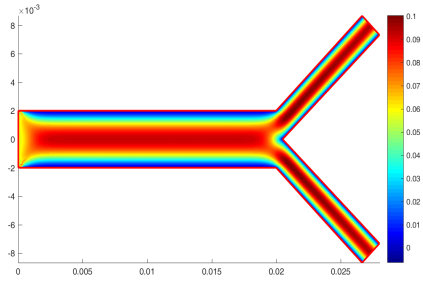

(d) Velocity magnitude for $\gamma = 1$, $Re = 200$ at approximately $4/4$ of cardiac cycle

Figure 7.22: Velocity Profiles for $\gamma = 1$ for different phases of cardiac cycle. In this figure, x axis indicates vessel lenght (m), y axis lumen diameter (m), and the colorbar indicates velocity magnitudes (m/s).

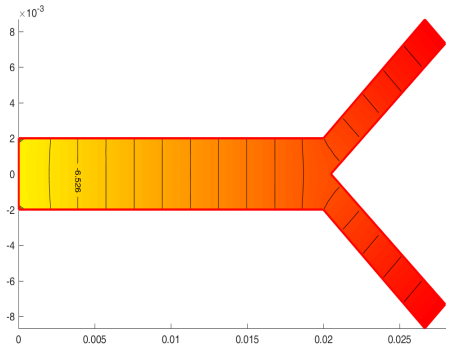

(a) Pressure profile for $\gamma = 1$, $Re = 200$ at approximately $1/4$ of cardiac cycle

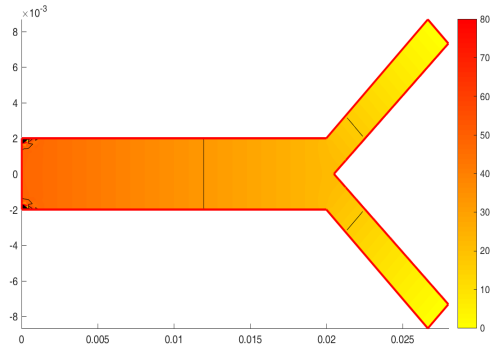

(b) Pressure profile for $\gamma = 1$, $Re = 200$ at approximately $2/4$ of cardiac cycle

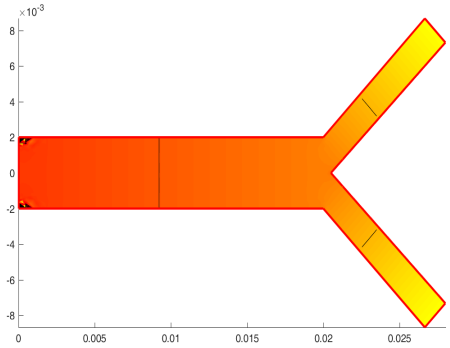

(c) Pressure profile for $\gamma = 1$, $Re = 200$ at approximately $3/4$ of cardiac cycle

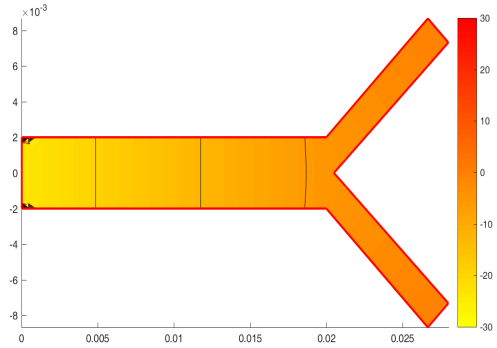

(d) Pressure profile for $\gamma = 1$, $Re = 200$ at approximately $4/4$ of cardiac cycle

Figure 7.23: Pressure profiles for $\gamma = 1$ for different phases of cardiac cycle. In this figure, x axis indicates vessel lenght (m), y axis lumen diameter (m), and the colorbar indicates pressure values (Pa).

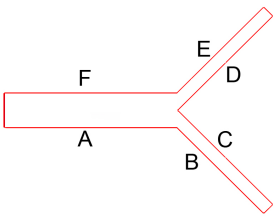

Figure 7.24: The wall labels of the geometry to indicate where the WSS values belong to in Figure 7.25

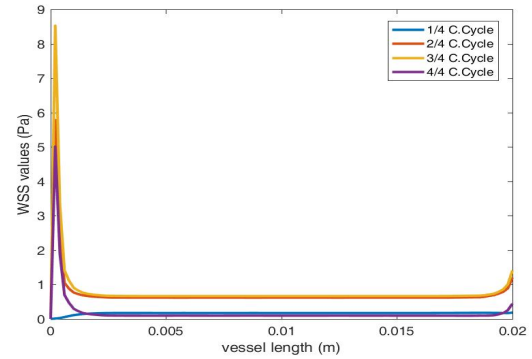

(a) WSS values at wall A

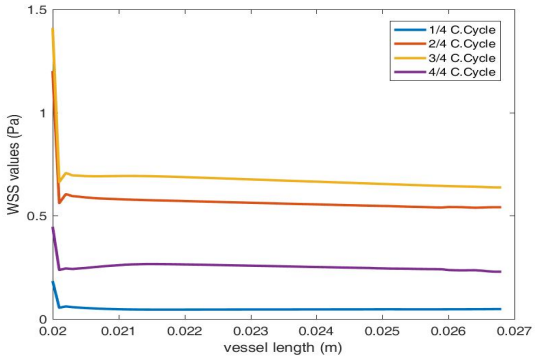

(b) WSS values at wall B

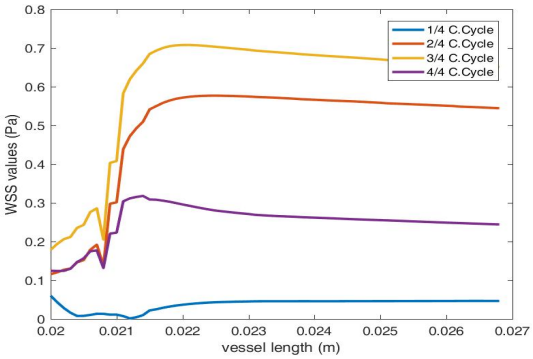

(c) WSS values at wall C

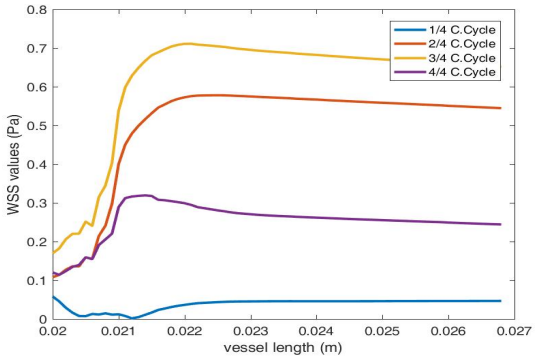

(d) WSS values at wall D

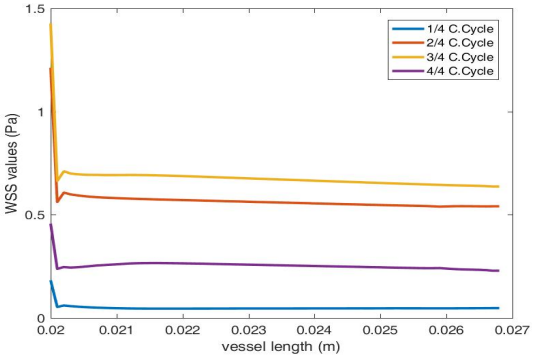

(e) WSS values at wall E

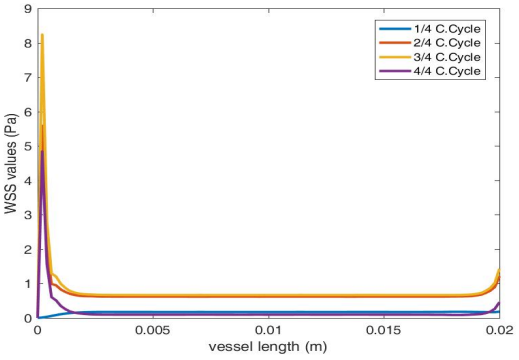

(f) WSS values at wall F

Figure 7.25: WSS values for $\gamma = 1$ for different phases of cardiac cycle for different walls of the artery.

- Figure 7.22c and 7.23c represent the beginning of the systole. In that phase, maximum velocity at the inlet occurs due to the contraction of the ventricles. Figure 7.22a and Figure 7.23c represent the beginning of diastole. In this phase, minimum velocity at the inlet occurs since ventricles are relaxed.

- One can observe from Figure 7.22a that, once the velocity becomes zero, back flow and vortex occurs due to the energy in the system (also see stagnant points in 7.25c and 7.25d). As the flow continues through the systolic phase, the energy is distributed inside, and this yields regular flows, seen in Figure 7.22b, 7.22c and 7.22d. In Figure 7.22c, high flow rate is apparent through the inlet at the systolic phase.

- Observing from Figure 7.22b, 7.22c and 7.22d, it takes time for flow to develop due to the inlet velocity profile. After it is developed, the regions close to the boundary forms a boundary layer to adapt the no slip boundary condition.

- After the branch, the maximum velocity at branching vessels are more than the main vessel due to the less diameter of the lumen.

- Observing from Figure 7.25a and 7.25f, we can see that the WSS is decreased to a stabilized level until the flow is fully developed. After development, it becomes stable through the branching region.

- In Figure 7.25b and 7.25e, we observe a decrease in wall shear stress values and stabilize through the outlet for walls B and E.

- In Figure 7.25b and 7.25e, we observe low wall shear stress values around the bifurcation. It a increases and stabilize through the outlet for walls C and D.

CHAPTER 8

CONCLUSIONS

This thesis aims to study two main goals, first is to give a numerical algorithm to solve Navier-Stokes equations governing the blood motion, and second is to investigate its feasibility on the cardiovascular system. For the first goal, we present grad-div stabilized fully discrete Navier-Stokes equations with backward Euler's method and present its stability and error analysis, and discuss existence and uniqueness of the approximate solutions. For the second goal, we present its numerical simulations such as stenosis, aneurysm and some other possible cases in cardiovascular system, since the effect of grad-div stabilization on the cardiovascular system has not been investigated in the literature. To understand its effect on cardiovascular system, we use the information from velocity and pressure fields, together with wall-shear stress values. Pulsatile nature of blood flow is also considered and the effect of grad-div stabilization parameter is investigated.

In our study, we find that

- Grad-div stabilized Navier-Stokes equations with backward Euler's method is unconditionally stable, and it admits a unique solution.
- With regularity assumptions, the error is bounded, thus the algorithm is convergent.
- The method provides observable mass conservation. In stenosis geometry, it allows to observe the results for higher Reynolds numbers than of without any stabilization.
- The stabilization allows to observe stenosis for higher severities.

Since the method suggests observable improvement in our applications in the cardiovascular system, it is promising for future studies. In [37], the study suggest that the grad-div stabilization allows more stable simulations in case of turbulent flows. For higher Reynolds numbers such as aorta at the systolic phase, turbulence partially occurs in cardiovascular system, and effect of grad-div stabilization should be investigated in such cases. In [4], the researchers study a branching vessel for different angles of bifurcation, and another study should be conducted on the effect of stabilization for different angles of branches, especially for higher angles since they are more susceptible for turbulence.

As a future research, a higher order algorithm, such as grad-div stabilized Navier-Stokes equations with Crank-Nicolson method should also be implemented and its effect on cardiovascular system should also be investigated. Finally, more complex geometries in cardiovascular system, such as more sudden expanding stenosis, or a branching artery for higher bifurcation angles should be investigated.

REFERENCES

[1] World Health Organization. (2017, May 17). *Cardiovascular diseases (CVDs)*. Retrieved from: https://www.who.int/en/news-room/fact-sheets/detail/cardiovascular-diseases-(cvds).

[2] L. Formaggia, A. Quarteroni, A. Veneziani. *Cardiovascular Mathematics Modeling and simulation of the circulatory system*. Springer-Verlag: Italia, Milano, 2009.

[3] V. John. *Finite Element Methods for Incompressible Flow Problems*. Springer Series in Computational Mathematics 51, Springer-Verlag: Berlin, 2016.

[4] O. Arjmandi-Tash, S.E. Razavi, R. Zanbouri, *Possibility of atherosclerosis in an arterial bifurcation model*. Bioimpacts. 1(4):225-8 , 2011.

[5] R.S. Reneman, A.P. Hoeks. *Wall shear stress as measured in vivo: consequences for the design of the arterial system*. Medical & Biological Engineering & Computing, 46(5):499–507, 2008.

[6] R.H. Anderson, R. Razavi, A.M. Taylor. *Cardiac anatomy revisited*. Journal of Anatomy, 205(3):159–177, 2004.

[7] A.J. Weinhaus, K.P. Roberts. *Anatomy of the human heart*. In Handbook of Cardiac Anatomy, Physiology, and Devices: Second Edition, 51-79, Humana Press: Totowa, NJ, 2005.

[8] F. Shaffer, R. McCraty, C.L. Zerr. *A healthy heart is not a metronome: an integrative review of the heart's anatomy and heart rate variability*. Frontiers in Psychology, 5(1040): 1-19 ,2014.

[9] F. Sotiropoulos, T.B. Le, A. Gilmanov. *Fluid mechanics of heart valves and their replacements*. Annual Review of Fluid Mechanics, 48(1):259-283, 2016.

[10] R.B. Hinton, K.E. Yutzey. *Heart valve structure and function in development and disease*. Annual Review of Physiology, 73: 29 – 46, 2011.

[11] S. Magder. *The meaning of blood pressure*. Crit. Care, 22: 257, 2018.

[12] J.L. Vincent. *Understanding cardiac output*. Crit Care, 12:174-174, 2008.

[13] J. Pinnell, S. Turner, S. Howell, *Cardiac muscle Physiology*. Continuing Education in Anaesthesia Critical Care & Pain, 7(3):85–88 , 2007.

[14] V.N. Barros, *The heart cycle: Review*. MOJ Womens Health, 8(1):66-69,2019.

[15] B.N. Baeyens, B. Chirosree, G.C. Brian, Y. Sanguk, A.S. Martin. *Endothelial fluid shear stress sensing in vascular health and disease*. The Journal of Clinical Investigation, 126(3):821-828, 2016.

[16] N.F. Renna, R. Garcia, J. Ramirez, R. M. Miatello. *Vascular repair and remodelling : A Review*. Physiologic and Pathologic Angiogenesis, IntechOpen Ch.11, 2017.

[17] N. Filipovic, M. Rosic, V. Isailovic, Z. Milosevic, D. Nikolic, D. Milašinović, M. Radovic, B. Stojanovic, M. Ivanovic, I. Tanaskovic, I. Saveljic, M. Milosevic, D. Petrovic, M. Nikolic, E. Themis, A. Sakellarios, P. Siogkas, P. Marraccini, F. vozzi, M. Kojic. *ARTREAT project: Computer, experimental and clinical analysis of three-dimensional plaque formation and progression in arteries*. Journal of the Serbian Society for Computational Mechanics, 5:129-146, 2015.

[18] M. Granér. *Determinants of coronary and carotid atherosclerosis in Finnish patients with clinically suspected coronary artery disease*. M.D. Thesis, Department of Medicine, Division of Cardiology Helsinki University Central Hospital Helsinki, Finland, 10: 1-118. 2007.

[19] J. Peiro, L. Formaggia, M. Gazzola, A. Radaelli, V. Rigamonti. *Shape reconstruction from medical images and quality mesh generation via implicit surfaces*. International Journal for Numerical Methods in Fluids, 53:1339 - 1360, 2007.

[20] A. Quarteroni. *What mathematics can do for the simumation of blood flow circulation*. AMS Subject Classification: 92C50, 96C10, 76Z05, 74F10, 65N30, 65M60, 2006.

[21] E. M. Cherry, J. K. Eaton *Shear thinning effects on blood flow in straight and curved tubes*. Phys. Fluids, 25(7), 073104, 2013.

[22] L. Lanotte, J. Mauer, S. Mendez, D.A. Fedosov, J.M. Fromental, V. Clavería, F. Nicoud, G. Gompper, M. Abkarian, *A new look at blood shear-thinning*. arXiv e-print: 1608.03730, 2016.

[23] A. Quarteroni, *Cardiovascular Mathematics*. Springer-Verlag: Italia, Milano, 2009.

[24] S.S. Dhawan, R.P.A. Nanjundappa, J.R. Branch, W.R. Taylor, A.A. Quyyumi, H. Jo, M.C. McDaniel, J. Suo, D. Giddens, H.Samady. *Shear stress and plaque development*. Expert Rev Cardiovasc Ther. 8(4), 545-56 , 2010.

[25] R.M. Lancellotti, C.L. Vergara, L. Valdettaro, S. Bose, A. Quarteroni. *Large eddy simulations for blood dynamics in realistic stenotic carotids*. Int. J. Numer. Meth. Biomed. Engng., 33(11), 2017.

[26] A. Quarteroni. *Numerical Models for Differential Problems*. Springer-Verlag: Italia, 2014.

[27] W. Layton. *An Introduction to the Numerical Analysis of Incompressible Viscous Flows*. SIAM, Philadelphia, PA, 2008.

[28] F. Bengzon, M. G. Larson. *The Finite Element Method: Theory, Implementation, and Applications*. Springer Publishing Company, Incorporated, 2013.

[29] B. Radi, A. ELHami. *Finite Volume Methods*. 10.1002/9781119492238.ch5, 2018.

[30] J. Peiró, J.S. Sherwin. *Finite Difference, Finite Element and Finite Volume Methods for Partial Differential Equations*. In: Yip S. (eds), Handbook of Materials Modeling, Springer, Dordrechtpp, 2415-2446, 2005.

[31] J. Donea, A. Huerta. *Finite Element Methods for Flow Problems*. John Wiley & Sons, Ltd, 2003.

[32] M.D. Gunzburger. *Finite Element Methods for Viscous Incompressible Flows: A Guide to Theory, Practice, and Algorithms*. Academic Press, Boston, 1989.

[33] L. P. Franca, T.J.R. Hughes. *Two classes of mixed finite element methods*. Computer Methods in Applied Mechanics and Engineering, 69(1):89–129, 1988.

[34] E.W. Jenkins, V. John, A. Linke, L.G. Rebholz. *On the parameter choice in grad-div stabilization for the Stokes equations*. Adv. Comput. Math., 40, 491–516, 2014.

[35] M.A. Olshanskii. *A low order Galerkin finite element method for the Navier-Stokes equations of steady incompressible flow: a stabilization issue and iterative methods*. Comput. Methods Appl. Mech. Engrg., 191, 5515–5536, 2002.

[36] J.D. Frutos, B. García-Archilla, V. John, J. Novo. *Grad-div stabilization for the evolutionary Oseen problem with inf-sup stable finite elements*. Journal of Scientific Computing, 66(3): 991-1024, 2016.

[37] J.D. Frutos, B. García-Archilla, V. John, J. Novo. *Analysis of the Grad-Div Stabilization for the Time-Dependent Navier–Stokes Equations with Inf-Sup Stable Finite Elements*. Advances in Computational Mathematics, 44(1): 195–225, 2017.

[38] W. Layton, C.M. Carolina, N. Monika, M. Olshanskii, L.G. Rebholz. *On the accuracy of rotation form in simulations*. Journal of Computational Physics, 128(9): 3433-3447, 2009.

[39] K. J. Galvin, A. Linke, L.G. Rebholz, N.E. Wilson, *Stabilizing poor mass conservation in incompressible flow problems with large irrotational forcing and application to thermal convection*. Computer Methods in Applied Mechanics and Engineering, 237-240:166-176, 2012.

[40] M.A. Case, V.J. Ervin, A. Linke, L.G. Rebholz. *A Connection Between Scott–Vogelius and Grad-Div Stabilized Taylor–Hood FE Approximations of the Navier–Stokes Equations*. SIAM J. Numer. Anal., 49(4), 1461–1481, 2011.

[41] J. G. Heywood, R. Rannacher. *Finite element approximation of the nonstationary Navier-Stokes problem, part II: Stability of solutions and error estimates uniform in time*. SIAM J. Numer. Anal., 23(4), 750–777, 1986.

[42] V. Girault, P.A. Raviart. *Finite element methods for Navier-Stokes equations: Theory and Algorithms*. Springer-Verlag, 1986.

[43] F. Hecht. *New development in FreeFem++*. *Journal of Numerical Mathematics*. 20, No 3-4, 251-266, 2012.

[44] A. Bozhok, G. Formato , C. Sad´ee , M. Mandic, P. Iliev, J. Ukwizagira. *Patient-specific blood flow modelling*. European Consortium for Mathematics in Industry, 28th ECMI Modelling Week Final Report, 19-26 July, Portugal, Lisboa, 2015.

[45] A. Buradi, A. Mahalingam. *Effect of Stenosis Severity on Wall Shear Stress Based Hemodynamic Descriptors using Multiphase Mixture Theory*. Journal of Applied Fluid Mechanics, 11(6), 1497-1509, 2018.

[46] V.A. Nosovitsky, O. J. Ilegbusi, J. Jiang, P. H. Stone, C. L. Feldman. *Effects of Curvature and Stenosis-Like Narrowing on Wall Shear Stress in a Coronary Artery Model with Phasic Flow, Computers and Biomedical Research*. 30(1), 61-82, 1997.

[47] Md. S. Rana, Md. F. Rubby, A.B.M.T. Hasan. *Study of Physiological Flow Through an Abdominal Aortic Aneurysm (AAA)*. Procedia Engineering, 105, 885-892, 2015.

[48] G.J. Sheard. *Flow dynamics and wall shear-stress variation in a fusiform aneurysm*. Journal of Engineering Mathematics, 64(4), 379–390, 2009.

[49] H.E. Salman, B. Ramazanli, M.M. Yavuz, H.C. Yalcin. *Biomechanical Investigation of Disturbed Hemodynamics-Induced Tissue Degeneration in Abdominal Aortic Aneurysms Using Computational and Experimental Techniques*. Frontiers in Bioengineering and Biotechnology, 7(111), 2019.

[50] C.M. Warboys, N. Amini, A. de Luca, P.C. Evans. *The role of blood flow in determining the sites of atherosclerotic plaques*. F1000 Med Reports, 3(5), 2011.

[51] R. Yamaguchi. *Flow structure and variation of wall shear stress in asymmetrical arterial branch*. Journal of Fluids and Structures, 13(4), 429-442, 1999.

[52] H. Fujii, R. Yamaguchi, K. Tanishita. *Distribution of Wall Shear Stress in Right-Angle Branches during Laminar Flow*. Jsme International Journal Series C-mechanical Systems Machine Elements and Manufacturing - JSME INT J C. 48, 468-476, 2005.

WEB REFERENCES

[53] Digital Image. *Heart Anatomy – Anatomy and Physiology*. https://opentextbc.ca/anatomyandphysiology/chapter/19-1-heart-anatomy/, accessed July 2019, licensed under CC BY 4.0.

[54] Digital Image. *Chambers and valves of the heart - Mayo Clinic*. https://www.mayoclinic.org/diseases-conditions/mitral-valve-regurgitation/multimedia/img-20110853, accessed August 2019, all rights reserved.

[55] Digital Image. *Pulmonary vs Systemic Circulation - Difference Guru*. https://difference.guru/difference-between-pulmonary-and-systemic-circulation/, accessed September 2019, public domain.

[56] Digital Image. *Systolic Vs. Diastolic Blood Pressures: 8 Major Differences*. https://vivadifferences.com/systolic-vs-diastolic-blood-pressures/, accessed September 2019, public domain.

[57] Digital Image. *Cardiac Action Potentials*. http://www.nataliescasebook.com/tag/cardiac-action-potentials, accessed October 2019, public domain.

[58] Digital Image. *Cardiac cycle*. https://en.wikipedia.org/wiki/Cardiac_cycle, accessed August 2019, licensed under CC BY-SA 4.0.

[59] Digital Image. *Vascularization by Miranda Goldman, Jemima Lamothe, Brittany Forkus, and Julia Tomaszweski*. https://openwetware.org/wiki/Vascularization_by_Miranda_Goldman,_Jemima_Lamothe,_Brittany_Forkus,_and_Julia_Tomaszweski, accessed August 2019, licensed under CC BY-SA 4.0.

[60] Digital Image. *Structure and Function of Blood Vessels - Anatomy and Physiology*. https://opentextbc.ca/anatomyandphysiology/cha

pter/20-1-structure-and-function-of-blood-vessels/, accessed August 2019, CC BY 4.0.

[61] Digital image from *The Emerging Concept of Vascular Remodeling,* by G.H. Gibbons and V. J. Dzau, 1994, the new england journal of medicine, 330(20):1431-1438.

[62] Digital Image. *Antibodies could stop heart disease, study finds*. https://www.sandiegouniontribune.com/business/biotech/sdut-heart-leeper-cd47-antibodies-2016jul20-story.html, accessed August 2019, licensed under Wikimedia Commons.

[63] Digital Image. *Representation of saccular (a) and fusiform (b)aneurysms*. https://www.researchgate.net/figure/Representation-of-saccular-a-and-fusiform-b-aneurysms_fig2_235363631, accessed August 2019, public domain.

[64] Digital Image. *The Ketchup Conundrum and Molecular Dynamics: Unraveling the Mystery of Shear Thinning*. https://softbites.org/2018/12/05/the-ketchup-conundrum-and-molecular-dynamics-unraveling-the-mystery-of-shear-thinning/, accessed August 2019, public domain.

[65] Digital Image. *Fahraeus-Lindqvist effect*. https://en.wikipedia.org/wiki/F%C3%A5hr%C3%A6us_effect, accessed August 2019, licensed under CC BY-SA 4.0.

[66] Digital image from *Pulsatile hemodynamics in patient-specific thoracic aortic dissection models constructed from computed tomography angiography.,* by J.K. Long Ko, R.W. Liu, D. Ma, L. Shi, S.C. Ho Yu and D. Wang, 2017, Journal of X-Ray Science and Technology, 25(2):233-245.